Available online at www.sciencedirect.com
ScienceDirect
Journal of Sound and Vibration 325 (2009) 297–320
JOURNAL OF SOUND AND VIBRATION
www.elsevier.com/locate/jsvi

Efficiency of targeted energy transfers in coupled nonlinear oscillators associated with 1:1 resonance captures: Part II, analytical study

T.P. Sapsis[a], A.F. Vakakis[b,c,d], O.V. Gendelman[e], L.A. Bergman[d,*], G. Kerschen[f], D.D. Quinn[g]

[a]*Department of Mechanical Engineering, Massachusetts Institute of Technology, USA*
[b]*Department of Applied Mathematical and Physical Sciences, National Technical University of Athens, Greece*
[c]*Department of Mechanical and Industrial Engineering, University of Illinois at Urbana-Champaign, USA*
[d]*Department of Aerospace Engineering, University of Illinois at Urbana-Champaign, USA*
[e]*Faculty of Mechanical Engineering, Technion—Israel Institute of Technology, Israel*
[f]*Aerospace and Mechanical Engineering Department (LTAS), Université de Liège, Belgium*
[g]*Department of Mechanical Engineering, The University of Akron, USA*

Received 13 March 2008; received in revised form 27 February 2009; accepted 4 March 2009
Handling Editor: C.L. Morfey
Available online 5 April 2009

Abstract

We study targeted energy transfer in a two degree-of-freedom damped system under the condition of 1:1 transient resonance capture. The system consists of a linear oscillator strongly coupled to an essentially nonlinear attachment or nonlinear energy sink. In a companion paper [Quinn et al., Efficiency of targeted energy transfers in coupled nonlinear oscillators associated with 1:1 resonance captures: part I, *Journal of Sound and Vibration* 311 (2008) 1228–1248] we studied the underlying structure of the Hamiltonian dynamics of this system, and showed that for sufficiently small values of viscous damping, nonlinear damped transitions are strongly influenced by the underlying topological structure of periodic and quasiperiodic orbits of the Hamiltonian system. In this work direct analytical treatment of the governing strongly nonlinear damped equations of motion is performed through slow/fast partitions of the transient responses, in order to investigate analytically the parameter region of optimal targeted energy transfer. To this end, we determine the characteristic time scales of the dynamics that influence the capacity of the nonlinear attachment to passively absorb and locally dissipate broadband energy from the linear oscillator. Then, we prove that optimal targeted energy transfer is realized for initial energies close to the neighborhood of a homoclinic orbit of the underlying Hamiltonian system. We study analytically transient orbits resulting as perturbations of the homoclinic orbit in the weakly damped system, and show that this yields an additional slow-time scale in the averaged dynamics, and leads to optimal targeted energy transfer from the linear oscillator to the nonlinear energy sink in a single "super-slow" half-cycle. We show that at higher energies,

*Corresponding author.
E-mail addresses: sapsis@mit.edu (T.P. Sapsis), vakakis@central.ntua.gr, avakakis@uiuc.edu (A.F. Vakakis), ovgend@techunix.technion.ac.il (O.V. Gendelman), lbergman@uiuc.edu (L.A. Bergman), g.kerschen@ulg.ac.be (G. Kerschen), quinn@uakron.edu (D.D. Quinn).

0022-460X/$ - see front matter
doi:10.1016/j.jsv.2009.03.004

this "super-slow" half-cycle is replaced by strong nonlinear beats, which lead to significant but suboptimal targeted energy transfer efficiency. Finally, we investigate numerically targeted energy transfer efficiency in this system over a wide range of system parameters and verify the analytical predictions.

1. Introduction

The aim of this work is to investigate conditions for optimal targeted energy transfer (TET), as judged by the strongest energy dissipation, in a two–degree-of-freedom (dof) nonlinear system under condition of 1:1 transient resonance capture (TRC) [1,2].

Previous works examined TET in systems of coupled nonlinear oscillators through energy exchanges between donor and acceptor discrete breathers due to nonlinear resonance [3–6]; resonant interactions between monochromatic electromagnetic waves and charged particles were studied, leading to chaotization of particles and transport in phase space. In Ref. [7] the processes governing energy exchange between coupled Klein–Gordon oscillators were analyzed; the same weakly coupled system was studied in Ref. [8] and it was shown that, under appropriate tuning, total energy transfer can be achieved for coupling above a critical threshold. In related works, localization of modes in a periodic chain with a local nonlinear disorder was analyzed [9]; transfer of energy between widely spaced modes in harmonically forced beams was analytically and experimentally studied [10]; and, in Ref. [11] a nonlinear dynamic absorber designed for a nonlinear primary was analyzed.

In this work, we consider the following weakly damped system,

$$\ddot{x} + \lambda_1\dot{x} + \lambda_2(\dot{x} - \dot{v}) + \omega_0^2 x + C(x - v)^3 = 0 \tag{1}$$

$$\varepsilon\ddot{v} + \lambda_2(\dot{v} - \dot{x}) + C(v - x)^3 = 0,$$

that is, a linear oscillator (LO), described by coordinate x, coupled to a lightweight, essentially nonlinear attachment, termed nonlinear energy sink—NES, described by coordinate v. The small parameter of the problem, $0 < \varepsilon \ll 1$, scales the mass of the NES.

This two-dof system possesses surprisingly complex dynamics [12,13]. Moreover, at certain ranges of parameters and initial conditions passive targeted energy transfer—TET—is possible, whereby vibration energy initially localized in the LO gets passively transferred to the lightweight attachment in a one-way irreversible fashion where it is locally dissipated without "spreading back" to the LO.

In Part I [14] the topological features of the corresponding Hamiltonian dynamics of system (1) (i.e., with no dissipative terms) were discussed. Focusing on an intermediate-energy region close to the 1:1 resonance manifold of the Hamiltonian dynamics the topological changes of intermediate-energy impulsive orbits (IOs) were studied [15] for varying energy. By IOs we denote periodic or quasi-periodic responses of the Hamiltonian system initiated with nonzero velocity for the LO and all other initial conditions zero. Specifically, it was found that above a critical value of energy, the topology of intermediate-energy IOs changes drastically, as these orbits make much larger excursions in phase space, resulting in continuous, strong energy exchanges between the LO and the NES, that appear in the form of strong nonlinear beats. It was also mentioned that this critical energy of the Hamiltonian system may be directly related to the energy threshold required for TET in the corresponding weakly damped system. Hence, a direct link between the Hamiltonian and weakly damped dynamics was established.

In the present work we revisit the intermediate-energy dynamics of the weakly damped system (1), in an effort to obtain conditions for realization of optimal TET from the LO to the NES. Since our study will be based on perturbation analysis, it will be necessarily restricted to the neighborhood of the 1:1 resonance manifold of the underlying Hamiltonian dynamics; hence, the damped dynamics will be studied under condition of 1:1 resonance capture. However, the ideas and techniques presented here can be extended to study optimal conditions for the more general case of m:n subharmonic TET.

First, we will review briefly some analytical results derived in Part I of this work [14] concerning the dynamics of the underlying Hamiltonian system. Subsequently, the topological structure of IOs will be presented with main emphasis given on their influence on TET efficiency. We will then proceed to the main part of this work, starting with the slow flow analysis of the governing equations through the complexification-averaging technique first developed by Manevitch [16]. This will be followed by qualitative analysis of the different mechanisms for TET in the system, and an analytical study of homoclinic perturbations in the weakly damped system. We will show that homoclinic perturbations yield an additional slow-time scale in the averaged dynamics which governs optimal TET from the LO to the NES occurring in a single "super-slow" half-cycle. The role of a homoclinic orbit on optimal TET was also discussed in Part I of this work [14] and in the work by Manevitch et al. [17]. We will conclude this work by providing numerical results of TET efficiency for a wide range of system parameters, which verify the analytical findings.

2. Some topological features of the dynamics

To initiate our analysis, we set $\omega_0^2 = 1$ in Eq. (1), and consider the damped dynamics close to the 1:1 resonance manifold of the Hamiltonian system. That is, assuming that the transient dynamics can be partitioned in terms of "slow" and "fast" components, we will consider damped oscillations with fast frequency approximately equal to the eigenfrequency of the LO, $\omega \approx 1$, in the form,

$$x(t) \approx \frac{a_1(t)}{\omega}\cos[\omega t + \alpha(t)], \quad v(t) \approx \frac{a_2(t)}{\omega}\cos[\omega t + \beta(t)], \tag{2}$$

where $a_1(t)$, $a_2(t)$ represent slowly varying amplitudes, and $\alpha(t)$, $\beta(t)$ slowly varying phases. Substituting Eq. (2) into Eq. (1) and averaging out all frequency components with fast frequencies higher than ω, we derive a system of four modulation equations governing the slow evolution of the amplitudes $a_1(t)$, $a_2(t)$ and phases $\alpha(t)$, $\beta(t)$ of the two oscillators; this defines the *slow flow* of system (1) in the neighbourhood of the 1:1 resonance manifold.

First we will make a small digression to discuss some features of the dynamics of the underlying Hamiltonian system obtained by setting $\lambda_1 = \lambda_2 = 0$ in Eq. (1). In Part I of this work [14] it was shown that the slow flow of the Hamiltonian system is fully integrable and can be reduced to the sphere $(R^+ \times S^1 \times S^1)$. Motivated by these results, we introduce the phase difference $\phi = \alpha - \beta$, the energy-like variable $r^2 = a_1^2 + (\sqrt{\varepsilon}a_2)^2$, and the angle $\psi \in [-\pi/2, \pi/2]$ defined by the relation $\tan[\psi/2 + \pi/4] = a_1/\sqrt{\varepsilon}a_2$. Considering the isoenergetic dynamical flow corresponding to $r = const$, the orbits of the corresponding Hamiltonian system lie an a topological 2-sphere, and follow the level sets of the first integral of motion.

Projections of the isoenergetic reduced Hamiltonian dynamics onto the unit disk at different energy levels are shown in Fig. 1. The north pole (NP) at $\psi = \pi/2$ lies at the center of the disk, while the south pole (SP) $\psi = -\pi/2$ is mapped onto the entire unit circle. In this projection, trajectories that pass through the SP approach the unit circle at $\phi = \pi/2$ and are continued at $\phi = -\pi/2$. If the response is localized to the LO, so

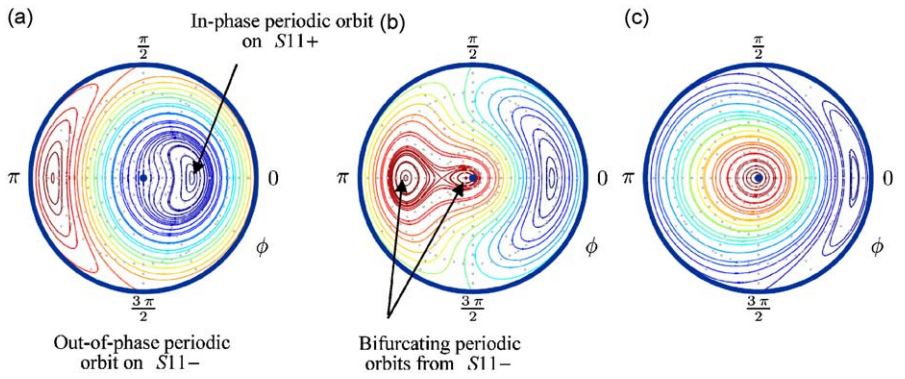

Fig. 1. Projection of the Hamiltonian dynamics of the isoenergetic manifold onto the unit disk at different energy levels ($\varepsilon = 0.1$, $C = 2/15$); (a) $r = 1.00$, (b) $r = 0.375$ and (c) $r = 0.25$.

that $a_2 \ll a_1$, the phase variable ψ lies close to $+\pi/2$. In contrast, a localized response in the nonlinear attachment (e.g, $a_1 \ll a_2$) implies that $\psi \approx -\pi/2$.

Equilibrium points of the slow-flow of the undamped system are explicitly evaluated by the following expressions,

$$\dot{\psi} = 0 \Rightarrow \sin\phi_{\mathrm{eq}} = 0 \Rightarrow \phi_{\mathrm{eq}} = 0, \pi$$

$$\dot{\phi} = 0 \Rightarrow \cos\psi_{\mathrm{eq}} = \frac{3\mathrm{Cr}^2}{8\varepsilon}(1+\varepsilon)^2[1-\sin(\psi_{\mathrm{eq}}+\gamma_{\mathrm{eq}})]\cos(\psi_{\mathrm{eq}}+\gamma_{\mathrm{eq}}),$$

with $\tan\gamma_{\mathrm{eq}} = 2\sqrt{\varepsilon}\cos\phi_{\mathrm{eq}}/(1-\varepsilon)$.

In general, equilibrium points with $\phi_{\mathrm{eq}} = 0$ correspond to in-phase periodic motions and have been denoted as $S11+$ in Ref. [13]. Those corresponding to $\phi_{\mathrm{eq}} = \pi$, represent out-of-phase periodic motions and have been denoted as $S11-$. In the phase space projections shown in Fig. 1, periodic motions on $S11+$ appear as equilibrium points on the horizontal axis to the right of the origin, whereas periodic motions on $S11-$ as equilibrium points on the horizontal axis to the left of the origin.

With increasing energy, i.e., as $r \to \infty$, both equilibrium points approach the asymptotic value,

$$\lim_{r\to\infty}\psi_{\mathrm{eq}} = \arctan((1-\varepsilon)/2\sqrt{\varepsilon}\cos\phi_{\mathrm{eq}}),$$

so that, for $0<\varepsilon\ll 1$, in the high-energy limit we have that $\psi_{\mathrm{eq},S11+}>0$ and $\psi_{\mathrm{eq},S11-}<0$. Hence, *with increasing energy the in-phase motion S11+ localizes to the LO, while the out-of-phase motion S11– localizes to the nonlinear attachment (the NES).*

Considering now the low-energy limit, it is easily shown that for sufficiently small values of r the equilibrium equation for ψ_{eq} leads to the simple limiting relation $\cos\psi_{\mathrm{eq}} \to 0$. Therefore, we conclude that as $r \to 0+$, the following are attained by the equilibrium values for ψ,

$$\lim_{r\to 0+}\psi_{\mathrm{eq},S11+} = -\pi/2 \quad \text{and} \quad \lim_{r\to 0+}\psi_{\mathrm{eq},S11-} = +\pi/2.$$

It follows that in the limit of small energies the in-phase periodic motion on $S11+$ localizes to the nonlinear attachment, whereas the out-of-phase periodic motion on $S11-$ to the LO. However, unlike the high-energy limits, as $r \to 0$ localization in this case is *complete* in either the LO or the nonlinear attachment.

In the transition from high to low energies, the out-of-phase branch of periodic motions $S11-$ undergoes two saddle-node bifurcations. In the first bifurcation, a new pair of stable–unstable equilibrium points is generated near $\psi = +\pi/2$. As energy decreases a second (inverse) saddle-node bifurcation occurs that destroys the unstable equilibrium generated in the first bifurcation together with the branch of $S11-$ that existed for higher energies (Fig. 1). It should be noted, however, that these bifurcations occur only below a certain critical mass ratio ε, i.e., only for sufficiently light attachments.

After this digression on the dynamics of the underlying Hamiltonian system, we next consider the weakly damped system (1) by rescaling the damping terms as, $\lambda_1 \to \varepsilon\lambda_1$, $\lambda_2 \to \varepsilon\lambda_2$, and expressing the slow flow equations in terms of the new variables r, ϕ and ψ. Then, we reduce the slow flow of the weakly damped system to the sphere $(r, \phi, \psi) \in (R^+ \times S^1 \times S^1)$,

$$\dot{r} = -\frac{r}{2}\{\varepsilon\lambda_1(1+\sin\psi) + \varepsilon\lambda_2[(1+\varepsilon)-(1-\varepsilon)\sin\psi - 2\varepsilon^{1/2}\cos\psi\cos\phi]\}$$

$$\dot{\psi} = \frac{-3\mathrm{Cr}^2}{8\varepsilon^{3/2}}[(1+\varepsilon)-(1-\varepsilon)\sin\psi - 2\varepsilon^{1/2}\cos\psi\cos\phi]\sin\phi - \frac{\varepsilon\lambda_1}{2}\cos\psi + \frac{\lambda_2}{2}[(1-\varepsilon)\cos\psi - 2\varepsilon^{1/2}\sin\psi\cos\phi]$$

$$\dot{\phi} = \frac{1}{2} - \frac{3\mathrm{Cr}^2}{16\varepsilon^2}[(1+\varepsilon)-(1-\varepsilon)\sin\psi - 2\varepsilon^{1/2}\cos\psi\cos\phi]\left[(1-\varepsilon) - 2\varepsilon^{1/2}\frac{\sin\psi\cos\phi}{\cos\psi}\right] - \varepsilon^{1/2}\lambda_2\frac{\sin\phi}{\cos\psi}. \quad (3)$$

We note that when $\lambda_1 = \lambda_2 = 0$ the slow-flow reduces to an integrable system on a two-torus [14]. For nonzero damping, however, the slow-flow dynamics is non-integrable and the dimensionality of the system Eq. (3) cannot be reduced further.

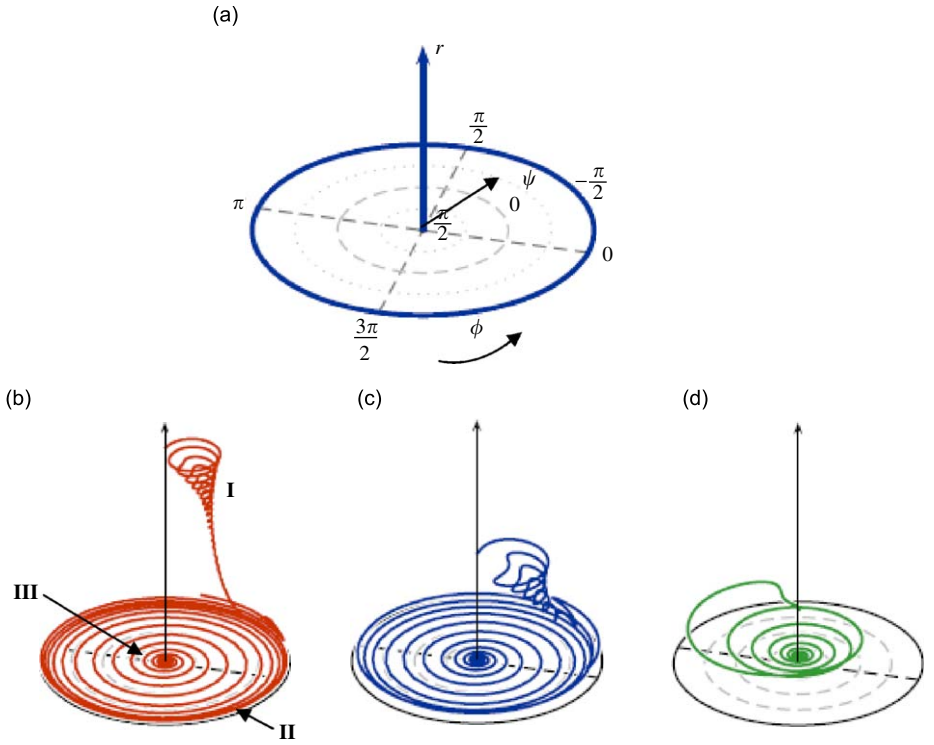

Fig. 2. Phase space projection of damped IOs for $\varepsilon = 0.1$, $C = 2/15$, and $\lambda_1 = \lambda_2 = 0.1$: (a) projection definition, (b) $r(0) = 2.0$, (c) $r(0) = 1.0$ and (d) $r(0) = 0.5$.

In Fig. 2 we depict projections of *IOs* of the weakly damped system (1) to the three-dimensional space $(r, \phi, \psi) \in (R^+ \times S^1 \times S^1)$ for three different initial energy levels. These results were obtained by performing direct numerical simulations of the damped system (1) subject to a single nonzero initial condition, namely the initial velocity of the LO (this is equivalent to applying an impulse to the LO with the system initially at rest, hence, the terminology [15]). The results of Fig. 2 can be directly compared to the plots of Fig. 1 depicting isoenergetic projections of the underlying Hamiltonian dynamics. In the damped case, however, instead of periodic orbits $S11\pm$ (or equivalently, equilibrium points of the slow flow) we get in-phase and out-of-phase decaying motions on the corresponding damped invariant manifolds [18,19]. These damped invariant manifolds can be considered as being analytical continuations for the weakly damped case of the invariant manifolds corresponding to periodic motions of $S11\pm$ of the Hamiltonian system. Their stability was discussed in Part I at Section 4.2 [14].

For the case of large initial energy (large impulse applied to the LO) there is an initial transient (Stage I in Fig. 2b) as the orbit gets attracted by the damped manifold $S11+$; this is followed by the slow evolution of the damped motion along $S11+$ as energy decreases with the motion predominantly localized to the NES as evidenced by the fact that $\psi(t) \approx -\pi/2$ (Stage II in Fig. 2b); finally, the damped manifold $S11+$ becomes unstable, and the dynamics makes a final transition to a weakly nonlinear (linearized) invariant manifold $S11-$ corresponding to out-of-phase oscillations being localized predominantly to the LO (as evidenced by the fact that $\lim_{t\to\infty}\psi(t) = \pi/2$—Stage III in Fig. 2b). In this case TET from the LO to the NES is realized predominantly during Stage I (TET through nonlinear beat) and Stage II (fundamental TET).

For lower initial energy (i.e., in the intermediate energy level) the initial transients of the dynamics during the attraction to $S11+$ possess larger amplitudes (Stage I, Fig. 2c) leading to an increase of the resulting TET due to nonlinear beats. In later times, Stages II and III of the dynamics are realized, similarly to the corresponding Stages in the higher-energy case. Compared to the previous case, TET is enhanced, especially during the initial transients of the motion where the LO and the NES undergo larger-amplitude nonlinear beats. However, qualitatively different dynamics is observed when the initial energy is further decreased.

As can be noted from the projection of Fig. 2d, the low-energy motion rapidly localizes to the LO as the dynamics approaches directly the weakly nonlinear (linearized) invariant manifold $S11-$, and, as a result, TET drastically diminishes. In essence, for this low energy value only Stage III of the dynamics is realized.

3. Conditions for optimal TET

In this Section we will investigate conditions for optimal TET in system (1). Our analytical derivations will be performed by rescaling the damping terms in system (1) according to $\lambda_1 = \lambda_2 = \varepsilon\lambda$ and considering again the normalized linear eigenfrequency $\omega_0^2 = 1$:

$$\ddot{x} + \varepsilon\lambda\dot{x} + \varepsilon\lambda(\dot{x} - \dot{v}) + x + C(x - v)^3 = 0$$

$$\varepsilon\ddot{v} + \varepsilon\lambda(\dot{v} - \dot{x}) + C(v - x)^3 = 0. \tag{4}$$

In similarity to the results of the previous Section we will consider initial conditions corresponding to excitation of an IO, i.e., $v(0) = \dot{v}(0) = x(0) = 0$ and $\dot{x}(0) = X$, and $0 < \varepsilon \ll 1$. This set of initial conditions is equivalent to forcing the LO with an impulse of magnitude X with the system originally at rest.

In Fig. 3 we depict the plot of instantaneous energy versus time of the system with $\varepsilon = 0.05$, $C = 1$ and $\varepsilon\lambda = 0.005$ for excitation of IOs at various energy levels (these parameter values will be assumed in the remainder of this Section, unless stated otherwise). This plot indicates the TET efficiency of the NES and the time scale of energy dissipation in the system. In accordance with previous findings reported in Part I of this work [14], we find that strong TET from the LO to the NES (as evidenced by rapid transient energy dissipation) is realized in the *intermediate energy region*, that is, in the neighborhood of the 1:1 resonance manifold of the dynamics of the underlying Hamiltonian system.

Moreover, *optimal TET*, as judged by the strongest energy dissipation in the plot of Fig. 3, is realized for initial impulses X (e.g., initial energies) in the range between the periodic IOs $U65$ and $U76$; it turns out [13] that these periodic IOs are close to the energy level of a saddle-node bifurcation of the linearized and strongly nonlinear components of the branch $S11-$ of out-of-phase periodic solutions of the underlying Hamiltonian system. At this energy level, an unstable hyperbolic periodic orbit is generated on the strongly nonlinear component of $S11-$. As shown below, it is the homoclinic orbit of this hyperbolic periodic orbit that affects the topology of nearby IOs and defines conditions for optimal TET in the weakly damped system.

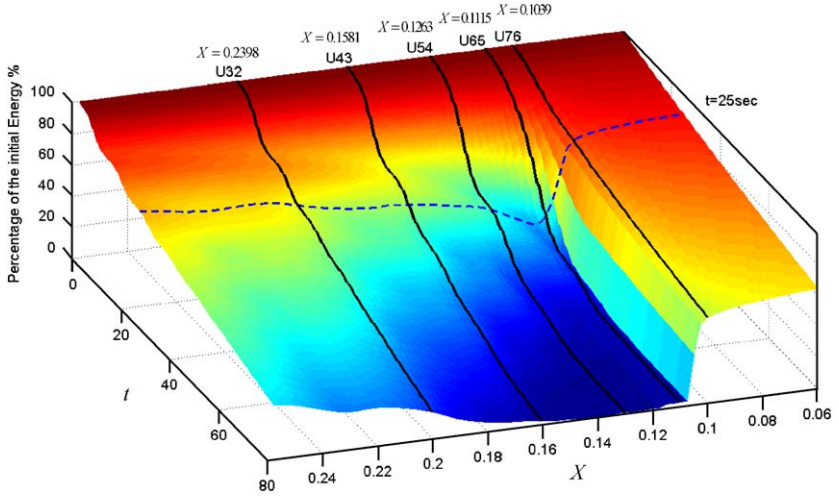

Fig. 3. Percentage of initial energy dissipated in system (4) when intermediate-energy damped IOs are excited ($\varepsilon = 0.05$, $C = 1$ and $\varepsilon\lambda = 0.005$): solid lines correspond to excitation of specific periodic IOs, and the dashed line indicates the instantaneous energy that remains in the system at $t = 25$ s.

3.1. Slow flow equations

The analytical study of conditions for optimal fundamental TET (i.e., TET under condition of 1:1 resonance capture between the LO and the NES) is carried out by applying the complexification-averaging technique to system (4) under condition of 1:1 internal resonance between the LO and the NES. As we shall see in the sequel, one of the main advantages of the above method compared to averaging is the formulation of the complete slow flow dynamics into a single complex integro-differential equation.

Only excitation of intermediate-energy IOs are considered, focusing to those lying close to the 1:1 resonance manifold at (fast) frequency $\omega \approx 1$. To this end, we introduce the new complex variables,

$$\psi_1(t) = \dot{v}(t) + \mathrm{j}v(t) \equiv \varphi_1(t)\mathrm{e}^{\mathrm{j}t}, \quad \psi_2(t) = \dot{x}(t) + \mathrm{j}x(t) \equiv \varphi_2(t)\mathrm{e}^{\mathrm{j}t},$$

where $\mathrm{j} = (-1)^{1/2}$. By these representations we partition the dynamics into slow (the complex amplitudes φ_1 and φ_2) and fast (the exponentials $\mathrm{e}^{\mathrm{j}t}$) components. Expressing the equations of motion (4) in terms of these complex variables, and applying averaging with respect to the fast-terms with frequency equal to unity or higher, we derive the following set of complex modulation equations governing the slowly varying complex amplitudes:

$$\begin{aligned} &\dot{\varphi}_1 + (\mathrm{j}/2)\varphi_1 + (\lambda/2)(\varphi_1 - \varphi_2) - (3\mathrm{j}C/8\varepsilon)|\varphi_1 - \varphi_2|^2(\varphi_1 - \varphi_2) = 0 \\ &\dot{\varphi}_2 + (\varepsilon\lambda/2)(2\varphi_2 - \varphi_1) + (3\mathrm{j}C/8)|\varphi_1 - \varphi_2|^2(\varphi_1 - \varphi_2) = 0. \end{aligned} \tag{5}$$

The corresponding initial conditions are given by $\varphi_1(0) = 0$ and $\varphi_2(0) = X$.

Introducing the new variables,

$$\left.\begin{aligned} u &= \varphi_1 - \varphi_2 \\ w &= \varepsilon\varphi_1 + \varphi_2 \end{aligned}\right\} \Leftrightarrow \left\{\begin{aligned} \varphi_1 &= (u + w)/(1 + \varepsilon) \\ \varphi_2 &= (w - \varepsilon u)/(1 + \varepsilon) \end{aligned}\right., \tag{6}$$

we express the system of modulation Eq. (5) as,

$$\begin{aligned} &\dot{u} + \frac{(1+\varepsilon)\lambda}{2}u - \frac{3(1+\varepsilon)\mathrm{j}C}{8\varepsilon}|u|^2u + \mathrm{j}\frac{u+w}{2(1+\varepsilon)} - \varepsilon\lambda\frac{w-\varepsilon u}{2(1+\varepsilon)} = 0 \\ &\dot{w} + \mathrm{j}\varepsilon\frac{u+w}{2(1+\varepsilon)} + \varepsilon\lambda\frac{w-\varepsilon u}{2(1+\varepsilon)} = 0, \end{aligned} \tag{7}$$

with initial conditions $u(0) = -X$ and $w(0) = X$. Variable u corresponds to the relative response between the LO and the NES, whereas w the (slow) motion of the center of mass of the system.

Hence, we have reduced the problem of studying intermediate-energy damped IOs of the initial system of coupled oscillators (4) under condition of 1:1 resonance capture, to the slow flow (Eq. (7)) of first order complex modulation equations which govern the slow flow close to the 1:1 resonance manifold. These equations are valid only for small- and moderate-energy IOs, i.e., for initial conditions $X < 0.5$ (cf. Fig. 3); the reason is that above this energy level the fast frequency of the response depends significantly on energy and the assumption $\omega \approx 1$ is violated.

Returning to the slow-flow Eq. (7), the second modulation equation can be solved explicitly as follows,

$$w(t) = X\mathrm{e}^{-\varepsilon(\mathrm{j}+\lambda t)/2} + \frac{\varepsilon(\varepsilon\lambda - \mathrm{j})}{2(1+\varepsilon)}\int_0^t \mathrm{e}^{-(\varepsilon/2)(\mathrm{j}+\lambda)[t-\tau]}u(\tau)\,\mathrm{d}\tau, \tag{8}$$

which, upon substitution into the first modulation equation yields the dynamical system:

$$\begin{aligned} \dot{u} - \frac{3\mathrm{j}C(1+\varepsilon)}{8\varepsilon}|u|^2u + \frac{\mathrm{j} + \lambda[\varepsilon^2 + (1+\varepsilon)^2]}{2(1+\varepsilon)}u = \frac{\varepsilon\lambda - \mathrm{j}}{2(1+\varepsilon)}X\mathrm{e}^{-\varepsilon(\mathrm{j}+\lambda)t/2} \\ + \varepsilon\left[\frac{(\varepsilon\lambda - \mathrm{j})}{2(1+\varepsilon)}\right]^2\int_0^t \mathrm{e}^{-(\varepsilon/2)(\mathrm{j}+\lambda)[t-\tau]}u(\tau)\,\mathrm{d}\tau, \quad u(0) = -X. \end{aligned} \tag{9}$$

This complex integro-differential equation governs the slow flow of a damped IO in the intermediate-energy regime, and it is equivalent to system (7). The above dynamical system, *which is formulated entirely in terms of*

the relative response u between the LO and the NES, provides information on the slow evolution of the damped dynamics close to the 1:1 resonance manifold and will be the basis of the following analytical derivations.

3.2. Analytical approximations of energy functionals in the slow flow

The study of optimal TET from the LO to the NES is directly related to the study of energy dissipation by the damper of the NES. This can be performed by analyzing the slow flow Eq. (9). The first step of our study is to derive expressions for the various energy measures in the system in terms of the complex modulations u and w. These expressions will be further exploited in an effort to study the dynamical features of these responses that yield conditions for optimal TET.

Hence, for the instantaneous total energy stored in the LO we derive the measure,

$$E_L(t) \equiv \frac{1}{2}[x^2(t)+\dot{x}^2(t)] \approx \frac{1}{2}[(\mathrm{Im}[\varphi_2 e^{jt}])^2 + (\mathrm{Re}[\varphi_2 e^{jt}])^2] = \frac{1}{2}|\varphi_2|^2 = \frac{|w-\varepsilon u|^2}{2(1+\varepsilon)^2}. \tag{10}$$

The instantaneous energy stored in the NES is approximately evaluated as,

$$\begin{aligned} E_{\mathrm{NL}}(t) &= \frac{1}{2}\left\{\varepsilon\dot{v}^2(t) + \frac{C}{2}[x(t)-v(t)]^4\right\} \approx \frac{1}{2}\left\{\varepsilon(\mathrm{Re}[\varphi_1 e^{jt}])^2 + \frac{C}{2}(\mathrm{Im}[u e^{jt}])^4\right\} \\ &= \frac{1}{2}\left\{\varepsilon\left(\mathrm{Re}\left[\frac{u+w}{1+\varepsilon}e^{jt}\right]\right)^2 + \frac{C}{2}(\mathrm{Im}[u e^{jt}])^4\right\}. \end{aligned} \tag{11}$$

Finally, the most important energy measure for our analysis will be the dissipation of energy due to the damper of the NES, approximated as,

$$\begin{aligned} E_{\mathrm{DISS}}(t) &= \int_0^t \varepsilon\lambda[\dot{x}(t)-\dot{v}(t)]^2\,\mathrm{d}t \approx \varepsilon\lambda\int_0^t (\mathrm{Re}[u e^{jt}])^2\,\mathrm{d}t \\ &= \varepsilon\lambda\int_0^t \{(\mathrm{Re}[u])^2\cos^2 t + (\mathrm{Im}[u])^2\sin^2 t - \mathrm{Re}[u]\mathrm{Im}[u]\sin 2t\}\,\mathrm{d}t \\ &= \varepsilon\lambda\int_0^t \left\{(\mathrm{Re}[u])^2\frac{1+\cos 2t}{2} + (\mathrm{Im}[u])^2\frac{1-\cos 2t}{2} - \mathrm{Re}[u]\mathrm{Im}[u]\sin 2t\right\}\mathrm{d}t. \end{aligned} \tag{12a}$$

Omitting terms with fast frequencies greater than unity from the integrand (this is consistent with our averaging analysis, based on averaging with respect to the fast frequency equal to unity), the above integral can be further approximated by the compact expression,

$$E_{\mathrm{DISS}}(t) \approx \frac{\varepsilon\lambda}{2}\int_0^t \{(\mathrm{Re}[u])^2 + (\mathrm{Im}[u])^2\}\,\mathrm{d}t = \frac{\varepsilon\lambda}{2}\int_0^t |u(t)|^2\,\mathrm{d}t. \tag{12b}$$

Hence, within the approximations of the analysis, the energy dissipated by the NES is directly related to the modulus of $u(t)$ which characterizes the relative response between the LO and the NES. It follows, that *enhanced TET in system* (4) *is realized when the modulus* $|u(t)|$ *exhibits large amplitudes, especially during the initial phase of motion where energy is at its highest.*

3.3. Qualitative analysis of different TET regimes

In Fig. 4 we present a typical solution of the dynamical system (7) depicting the slow flow of a damped IO in the upper intermediate-energy regime of Fig. 3. The initial "wiggles" in the slow-flow represent the initial attraction of the dynamics by the damped in-phase invariant manifold $S11+$, and correspond to initial nonlinear beats in the full response. As we will see, although short in duration, the energy dissipated by the NES in this initial nonlinear beat regime can be quite significant.

In Fig. 5 we examine the dynamics of the averaged system (7) (or equivalently Eq. (9)) over the entire intermediate-energy regime of damped IOs. Starting from relatively high energies (i.e., from the highest value of impulsive magnitude X, cf. Fig. 5a), the initial regime of nonlinear beats (corresponding to the attraction of

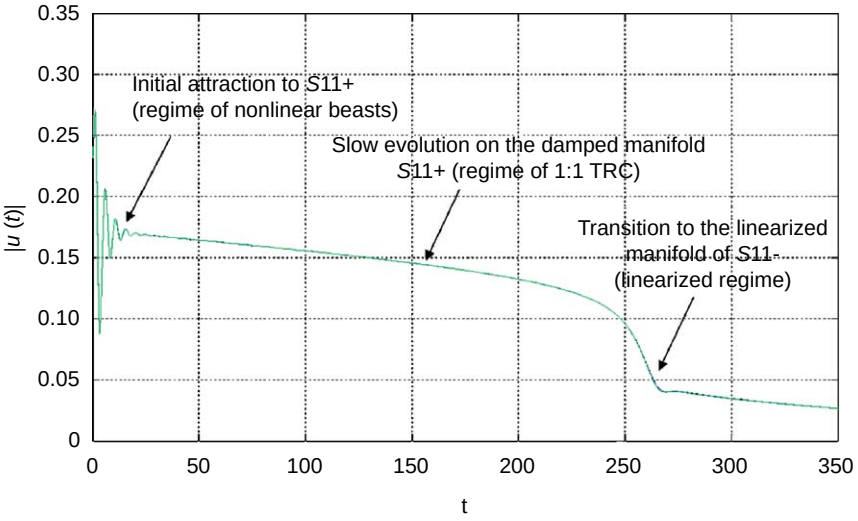

Fig. 4. Slow flow (7) of a damped IO in the intermediate-energy regime of Fig. 3.

the dynamics to the stable damped invariant manifold $S11+$) leads to strong energy exchanges between the LO and the NES; as the dynamics settles to the in-phase damped oscillation on $S11+$ the energy exchanges diminish and slow energy dissipation is realized in both oscillators; finally the dynamics makes the transition to the linearized damped manifold $S11-$ at the later stage of the response when nearly the entire energy of the system has been dissipated.

From the results depicted in the plots of Fig. 5 we conclude that in the upper region of the intermediate-energy regime TET is relatively weak as the impulsively excited LO retains most of its energy throughout the oscillation. As the impulsive energy decreases (cf. Figs. 5b and c) the initial regime of nonlinear beats expands and stronger energy exchanges between the impulsively forced LO and NES are realized; moreover, the dynamics instead of settling to $S11+$, undergoes a transition to the linearized manifold $S11-$. These features of the slow dynamics enhance TET in the system, as judged by the efficient dissipation of energy in both oscillators. However, optimal energy dissipation (and hence, TET) is realized in Fig. 5d, where the initial regime of beats is replaced by *a slow oscillation during which the entire energy of the LO gets transferred to the NES over* a *single half-cycle*. Some of this energy gets "backscattered" to the LO at a later stage through low-amplitude nonlinear beats, but the major amount of transferred energy to the NES gets dissipated during the initial half-cycle of energy transfer; this provides the *condition for optimal TET* in this system, and corresponds to the "ridge" in Fig. 3 realized at $X \approx 0.11$. However, even slight decrease of the impulsive magnitude X changes qualitatively the slow dynamics, as both oscillators now settle into out-of-phase linearized responses and negligible TET takes place; in this case the slow dynamics gets directly attracted by the linearized manifold $S11-$.

Hence, the slow dynamics of the damped IOs in the intermediate-energy regime is quite complex. Indeed, based on the qualitative features of the damped IO dynamics we may divide the intermediate-energy regime of Fig. 3 into three subregimes; these can be distinguished by the features of the slow-flow dynamics (Eq. (9)) during the initial, highly energetic stage of the impulsive motion where most TET is realized. In the *upper subregime* corresponding to higher impulsive magnitudes (cf. Figs. 5a–c), initial wiggles in the slow flow dynamics take place and TET is realized primary during the corresponding initial nonlinear beats. The *middle subregime* (cf. Fig. 5d) is the regime of optimal TET, and is governed by the most complex dynamics; the initial slow-flow dynamics is realized through a single "super-slow" half-cycle during which the entire energy of the LO is transferred to the NES. Hence, it appears that the initial nonlinear beats realized in the upper subregime degenerate to a single "super-slow" half-cycle of the slow-flow as the middle subregime is reached. As shown in the following analysis, the dynamic mechanism generating the "super-slow" degeneration of the slow dynamics in Fig. 5d is a homoclinic orbit of the unstable orbit on $S11-$ generated by the saddle-node bifurcation of branch $S11-$ [13]. Finally, the *lower subregime* is characterized by linearized motion

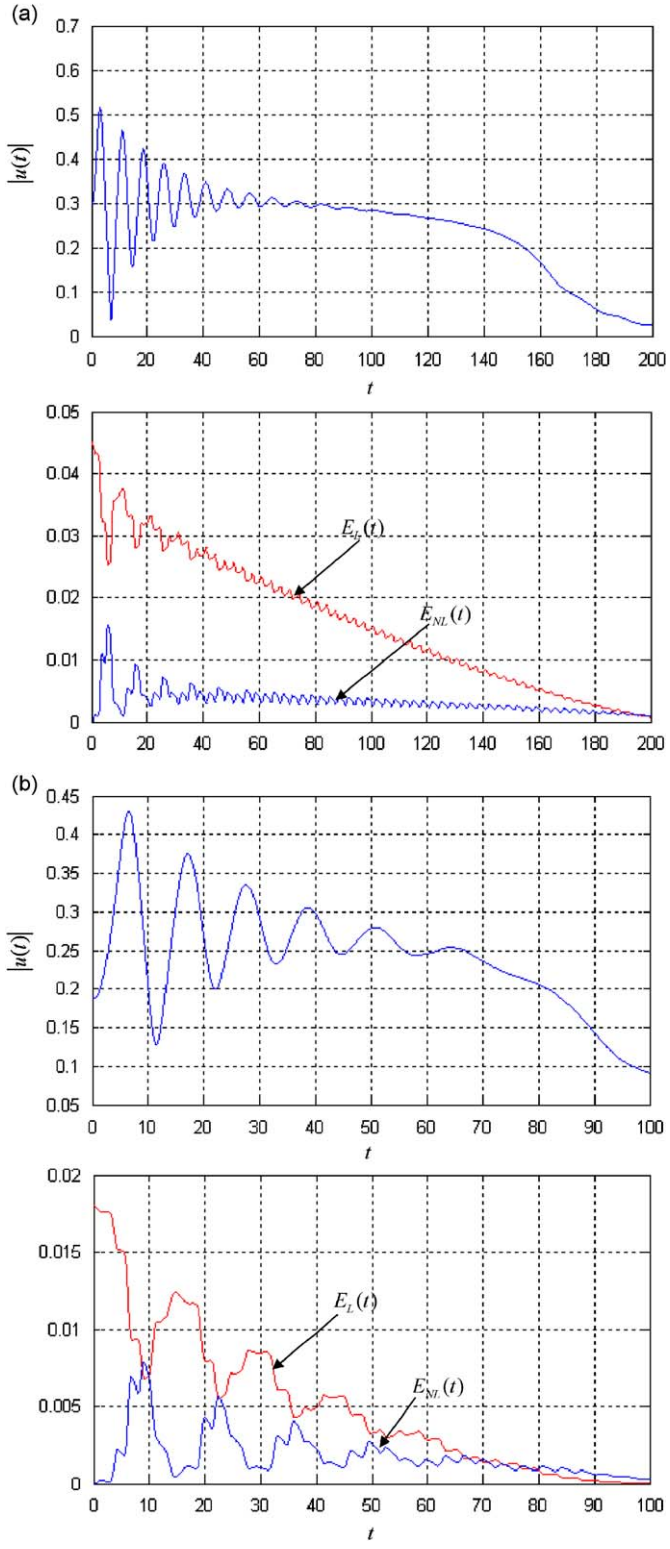

Fig. 5. Slow-flow (7) or (9) of damped IOs in the intermediate-energy regime: (a) $X = 0.30$ (upper regime), (b) $X = 0.19$, (c) $X = 0.12$, (d) $X = 0.11$ (optimal TET) and (e) $X = 0.09$ (lower regime).

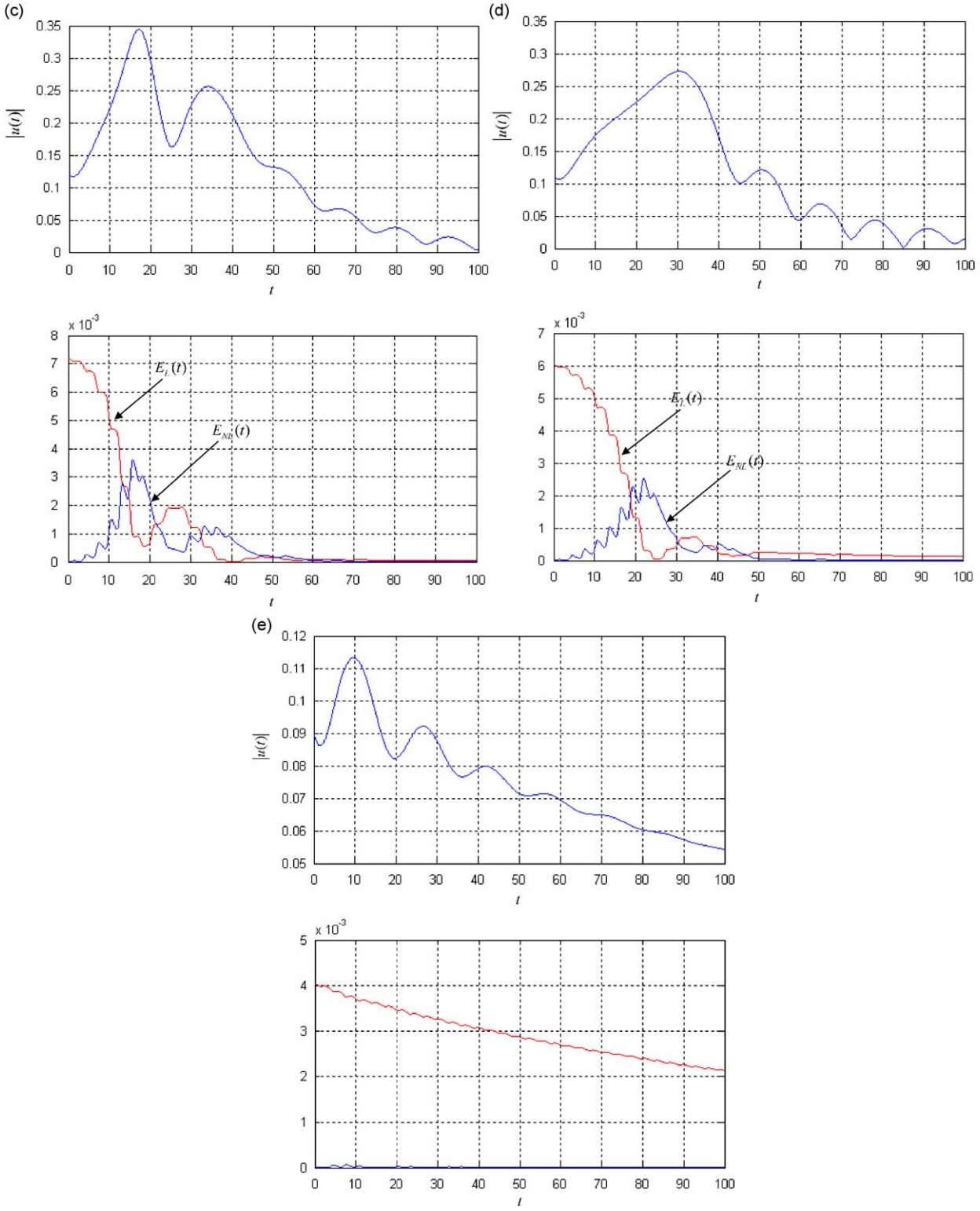

Fig. 5. (*Continued*)

predominantly localized to the LO, with complete absence on nonlinear beats and negligible TET. We note that the referred optimization of TET is not based on a formal optimization criterion, but rather on the qualitative argument that optimal TET corresponds to one-way transfer of nearly all of the energy of the LO to the nonlinear attachment in a single 'super-slow' half-cycle. This is caused by an additional 'super-slow' time scale in the dynamics which only exists in the neighborhood of the homoclinic orbit of the underlying Hamiltonian system.

3.4. Analytical study of the regime of optimal TET

The previous discussion and results provide ample motivation for focusing on the initial, highly energetic regime of the slow-flow dynamics [Eq. (7) or equivalently Eq. (9)], as this represents the most critical stage for TET. Hence, we consider the modulation Eq. (9) and *restrict the analysis to the initial stage of the dynamics*. Mathematically, we will be interested in the dynamics up to times of $O(1/\varepsilon^{1/2})$, for initial conditions (impulses) $X = O(\varepsilon^{1/2})$. Under these assumptions we consider the integral term on the right-hand-side of Eq. (9) and express it as

$$I \equiv \varepsilon\left[\frac{(\varepsilon\lambda - \mathrm{j})}{2(1+\varepsilon)}\right]^2 \int_0^t \mathrm{e}^{-(\varepsilon/2)(\mathrm{j}+\lambda)[t-\tau]} u(\tau)\,\mathrm{d}\tau = \varepsilon\left[\frac{1}{2(1+\varepsilon)}\right]^2 \int_0^t \mathrm{e}^{-(\varepsilon/2)(\mathrm{j}+\lambda)[t-\tau]} u(\tau)\,\mathrm{d}\tau + O(\varepsilon^2).$$

Assuming that $t = O(\varepsilon^{-1/2})$, we have also that $|\tau - t| = O(\varepsilon^{-1/2})$; it follows that by expanding the exponential in the integrand in Taylor series in terms of ε, the integral I can be approximated as,

$$I \approx \varepsilon\left[\frac{1}{2(1+\varepsilon)}\right]^2 \int_0^t u(\tau)\,\mathrm{d}\tau + O(\varepsilon^{3/2}),$$

or, by invoking the mean value theorem of integral calculus, as

$$I \approx 2^{-2}(1+\varepsilon)^{-2}\varepsilon t u(t_0),$$

for some t_0 in the interval $0 < t_0 < t$. Given that $t = O(\varepsilon^{-1/2})$ and $u(t_0) = O(X) = O(\varepsilon^{1/2})$, we prove that for times smaller than $O(\varepsilon^{-1/2})$, the integral is ordered as, $I = O(\varepsilon)$, and hence is a small quantity asymptotically as $\varepsilon \to 0$.

Taking this result into account, and introducing the variable transformations $u = \varepsilon^{1/2} z$ and $X = \varepsilon^{1/2} Z$ to account for the scaling of the initial condition (impulse) X, we express the modulation equation Eq. (9) in the form,

$$\dot{z} - \frac{3\mathrm{j}C}{8}|z|^2 z + \frac{\mathrm{j}+\lambda}{2} z = -\frac{\mathrm{j}Z}{2} + O(\varepsilon, \varepsilon^{1/2}\lambda), \quad z(0) = -Z, \;\; t \text{ up to } O(\varepsilon^{-1/2}), \tag{13}$$

where the variable z and initial condition Z are assumed to be $O(1)$ quantities, unless otherwise noted. Finally, introducing the rescalings,

$$z \to \left(\frac{4}{3C}\right)^{1/2} z, \quad w \to \left(\frac{4}{3C}\right)^{1/2} w,$$

the new notation,

$$B = -\left(\frac{3C}{4}\right)^{1/2} Z,$$

and the additional scaling for the damping coefficient, $\lambda = \varepsilon^{1/2}\hat{\lambda}$, the system is brought into the final form,

$$\dot{z} - \frac{\mathrm{j}}{2}|z|^2 z + \frac{\mathrm{j} + \varepsilon^{1/2}\hat{\lambda}}{2} z = \frac{\mathrm{j}B}{2} + O(\varepsilon), \quad z(0) = B, \;\; t \text{ up to } O(\varepsilon^{-1/2}). \tag{14}$$

All quantities in the above reduced slow flow equation except the small parameter ε are assumed to be $O(1)$. The complex modulation Eq. (14) provides an approximation to the initial slow-flow dynamics, and is valid formally up to times of $O(\varepsilon^{-1/2})$.

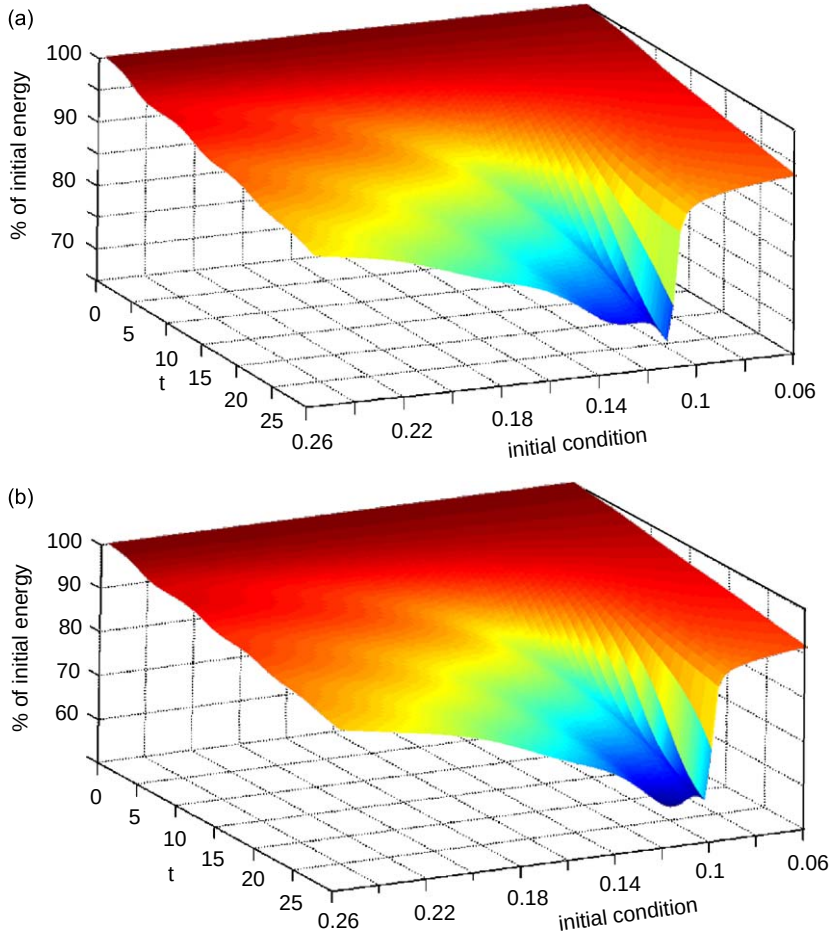

Fig. 6. Percentage of energy dissipated when intermediate-energy damped IOs are excited ($\varepsilon = 0.05$, $C = 1$ and $\lambda = \varepsilon^{1/2}\hat{\lambda} = 0.1$): (a) full slow-slow (7) or (9) and (b) approximation of the slow-flow (12) or (14) in the initial stage of the dynamics.

In Fig. 6 we test this approximation by comparing the slow flows resulting from the reduced model Eq. (13) or Eq. (14), to the full slow-flow Eq. (7) or Eq. (9). This is performed by computing the corresponding energy dissipation measures predicted by the two approximations when intermediate energy IOs are excited. This comparison clearly validates the slow flow approximation (Eq. (14)) in the intermediate-energy level of interest in our study.

Introducing the polar transformation $z = Ne^{j\delta}$, substituting into Eq. (14), and separating real and imaginary parts the reduced slow flow can be expressed in terms of the two real modulation equations,

$$\dot{N} + \frac{\varepsilon^{1/2}\hat{\lambda}}{2} N = \frac{B}{2} \sin\delta + O(\varepsilon), \quad N(0) = B$$

$$\dot{\delta} + \frac{1}{2} - \frac{1}{2} N^2 = \frac{B}{2N} \cos\delta + O(\varepsilon), \quad \delta(0) = 0. \tag{15}$$

These equations govern the slow evolutions of the amplitude N and phase δ of the complex modulation z of the damped IO, during the initial regime of the dynamics. Note that for $\hat{\lambda} = 0$ the system is integrable as is shown below.

In Fig. 7 we depict the initial regime of slow-flow dynamics for $\varepsilon = 0.05$, $\hat{\lambda} = 0.4472$ and three different normalized impulses (initial conditions) B. For B above the critical level $B_{cr}(\hat{\lambda} = 0.4472) \approx 0.3814$, the

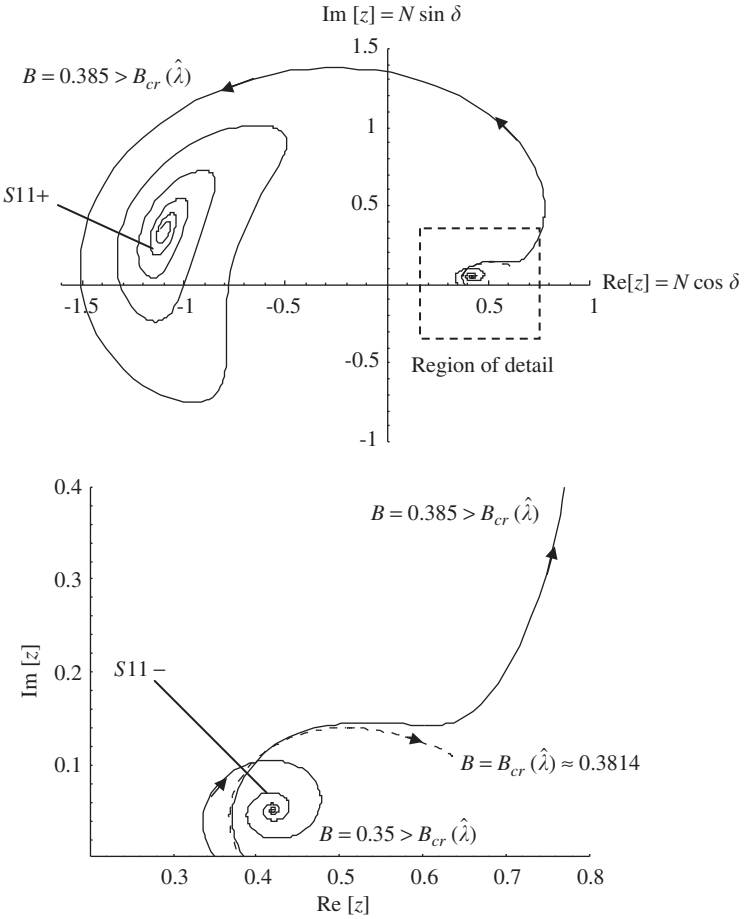

Fig. 7. Parametric plots of Im[z] against Re[z] with t being the parametrizing variable ($\hat{\lambda} = 0.4472$): initial regime of slow-flow dynamics of intermediate-energy damped IOs for different normalized impulses B [slow-flow (14) or (15)].

slow-flow model (14) predicts large excursion of the damped IO in phase space. In fact, after executing relatively large-amplitude transients, the orbit is attracted by the stable in-phase damped invariant manifold $S11+$; these initial transients correspond to the nonlinear beats (the "wiggles") observed in the initial stage of the full slow-flow model (9) in the upper subregime of the intermediate-energy regime (cf. Figs. 4 and 5a–c). Note, that since the slow flow model (14) and (15) is valid only for the initial stage of the slow-flow dynamics, it cannot predict the eventual transition of the dynamics from $S11+$ to $S11-$ in the later, low-energy (linearized) stage of the oscillation.

For B below the critical level $B_{\rm cr}(\hat{\lambda})$, there is a significant qualitative change in the dynamics as the IO executes small-amplitude oscillations and is being attracted by the out-of-phase damped invariant manifold $S11-$; this corresponds to the linearized dynamics realized in the lower subregime of the intermediate-energy range (cf. Fig. 5e).

The critical orbit that separates these two qualitatively different dynamics is a *perturbed homoclinic orbit* realized for $B = B_{\rm cr}(\hat{\lambda})$. This special orbit can be regarded as the damped perturbation of the homoclinic loop of the unstable undamped invariant manifold $S11-$ of the Hamiltonian system that is generated through a saddle-node bifurcation [13]. *This damped perturbed homoclinic orbit appears as the initial "super-slow" half-cycle* in the plot of Fig. 5d, and corresponds to the case of *optimal TET* in the system. In Fig. 7 we depict the portion of this damped homoclinic perturbation corresponding to the solution of the slow-flow dynamical systems (14) and (15) for the given initial conditions, i.e., $z(0) = B$. We note that these are peculiar forms of dynamical systems, as the initial conditions appear also as excitation terms on their right-hand-sides. In what

follows, the damped homoclinic perturbation will be analytically studied in an effort to analytically model the optimal TET regime depicted in Fig. 5d.

Reconsidering the slow flow system Eq. (14) or Eq. (15), we seek its solution in the *regular* perturbation form,

$$z(t) = z_0(t) + \varepsilon^{1/2}\hat{\lambda} z_1(t) + O(\varepsilon), \quad B = B_0 + \varepsilon^{1/2}\hat{\lambda} B_1 + O(\varepsilon). \tag{16}$$

Substituting into Eq. (14) and considering only $O(1)$ terms in the resulting expression we derive the system at the first order of approximation,

$$\dot{z}_0 - \frac{\mathrm{j}}{2}|z_0|^2 z_0 + \frac{\mathrm{j}}{2} z_0 = \frac{\mathrm{j} B_0}{2}, \quad z_0(0) = B_0, \tag{17a}$$

or, in terms of the polar transformation $z_0 = N_0 \mathrm{e}^{\mathrm{j}\delta_0}$,

$$\dot{N}_0 = \frac{B_0}{2}\sin\,\delta_0, \quad N_0(0) = B_0$$

$$\dot{\delta}_0 + \frac{1}{2} - \frac{1}{2N_0^2} = \frac{B_0}{2N_0}\cos\,\delta_0, \quad \delta_0(0) = 0. \tag{17b}$$

We note that due to scaling of the damping term in Eqs. (14) and (15), there are no dissipative terms in this first order of approximation. Damping effects enter into the problem at the next order of approximation.

It can be proved that the undamped slow-flow Eq. (17a) or Eq. (17b) is integrable, as it possesses the following Hamiltonian (first integral of the motion),

$$\frac{\mathrm{j}}{2}|z_0|^2 - \frac{\mathrm{j}}{4}|z_0|^4 - \frac{\mathrm{j} B_0}{2} z_0^* - \frac{\mathrm{j} B_0}{2} z_0 = h, \tag{18}$$

where the asterisk denotes complex conjugate. Taking into account the integrability of the system we can obtain a closed form (exact) solution. Indeed, taking into account Eq. (18) system (17b) reduces to the one-dimensional slow-flow,

$$2\dot{a} = [f(a; B_0)]^{1/2}, \quad f(a; B_0) \equiv 4B_0 a - \left(a - \frac{a^2}{2} + \frac{B_0^4}{2} + B_0^2\right)^2$$

$$\sin\delta_0 = \frac{2}{B_0}\frac{\mathrm{d}\sqrt{a}}{\mathrm{d}t}, \quad a(0) = B_0^2, \;\; \delta_0(0) = 0, \tag{19}$$

where we introduced the notation $a(t) \equiv N_0^2(t)$. The roots of the polynomial $f(a; B_0)$ depend on the parameter B_0 (cf. Fig. 8). For $B_0 > B_{0\mathrm{cr}} \approx 0.36727$ the polynomial $f(a; B_0)$ possesses two real distinct roots for a, whereas for $B_0 < B_{0\mathrm{cr}}$ it possesses four distinct real roots. For $B_0 = B_{0\mathrm{cr}}$ two of the real roots coincide, so $f(a; B_0)$ possesses only three distinct real roots. These are given by

$$a_1 = B_{0\mathrm{cr}} < a_2 = a_3 = 0.4563 < a_4 = 2.9525, \quad B = B_{0\mathrm{cr}} \approx 0.36727.$$

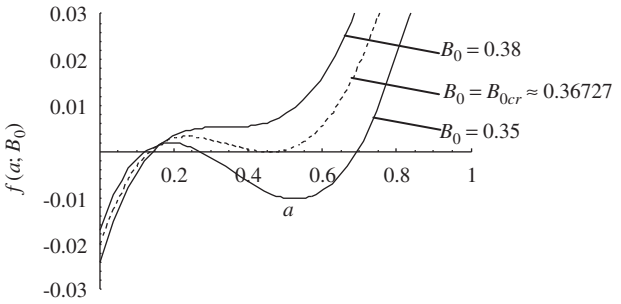

Fig. 8. Roots of $f(B_0, a) = 0$ (the additional real root for $a > 1$ is not shown).

It will be proven that for $B = B_{0\mathrm{cr}} \approx 0.36727$ system (19) possesses a homoclinic orbit, which we now proceed to compute explicitly.

Indeed, for $B_0 = B_{0\mathrm{cr}}$ the reduced slow-flow dynamical system (19) can be integrated by quadratures as,

$$\dot{a} = \frac{1}{4}[(a - B_{0\mathrm{cr}}^2)(a_2 - a)^2(a_4 - a)]^{1/2} \Rightarrow t = 4\int_{B_{0\mathrm{cr}}^2}^{a} \frac{\mathrm{d}\upsilon}{(a_2 - \upsilon)[(\upsilon - B_{0\mathrm{cr}}^2)(a_4 - \upsilon)]^{1/2}}, \tag{20}$$

where the initial condition $a(0) = B_{0\mathrm{cr}}^2$ was imposed, and it was recognized that $a(t) \geqslant B_{0\mathrm{cr}}^2$ for $t \geqslant 0$. We note that Eq. (20) provides the unique solution of the initial value problem (19). The definite integral in the expression above can be explicitly evaluated [20] to yield the analytical homoclinic orbit of the first-order system (17a) or (17b),

$$N_0^2(t) \equiv a_h^{(-)}(t) = a_2 - \frac{\gamma_1\gamma_2}{\gamma_1 \sinh^2\left(\frac{\sqrt{\gamma_1\gamma_2}}{8}t\right) + \gamma_2 \cosh^2\left(\frac{\sqrt{\gamma_1\gamma_2}}{8}t\right)} \tag{21a}$$

$$\delta_0(t) = \delta_{0h}^{(-)}(t) = \sin^{-1}\left[\frac{2}{B_{0\mathrm{cr}}}\frac{\mathrm{d}\sqrt{a_h^{(-)}(t)}}{\mathrm{d}t}\right]. \tag{21b}$$

In the expressions above we use the definitions, $\gamma_1 = a_2 - B_{0\mathrm{cr}}^2$, $\gamma_2 = a_4 - a_2$, and only the branch of the solution corresponding to $t \geqslant 0$ is selected. The solution (21) assumes the limiting values, $N_0(0) = B_{0\mathrm{cr}}$ and $\lim_{t\to+\infty} N_0(t) = \sqrt{a_2}$. Of course, this solution can be extended for $t<0$, but the resulting branch of the homoclinic orbit is not a solution of the initial value problem (17), and satisfies the alternative limiting relation $\lim_{t\to-\infty} N_0(t) = \sqrt{a_2}$.

We mention that the system (20) provides an additional homoclinic loop for Eq. (17) (which, however, does not satisfy the initial condition $a(0) = B_{0\mathrm{cr}}^2$), given by:

$$N_0^2(t) \equiv a_h^{(+)}(t) = a_2 + \frac{\gamma_1\gamma_2}{\gamma_1 \cosh^2\left(\frac{\sqrt{\gamma_1\gamma_2}}{8}t\right) + \gamma_2 \sinh^2\left(\frac{\sqrt{\gamma_1\gamma_2}}{8}t\right)} \tag{22a}$$

$$\delta_0(t) = \delta_{0h}^{(+)}(t) = \sin^{-1}\left[\frac{2}{B_{0\mathrm{cr}}}\frac{\mathrm{d}\sqrt{a_h^{(+)}(t)}}{\mathrm{d}t}\right]. \tag{22b}$$

This homoclinic loop correspond to the limiting values, $N_0(0) = \sqrt{a_4}$ and $\lim_{t\to\pm\infty} N_0(t) = \sqrt{a_2}$, and it will not be taken into account in the following analytical derivations.

In Fig. 9 the two homoclinic loops corresponding to Eqs. (21a,21b) and (22a,22b) are depicted. These loops are shown in dashed lines for the full range $-\infty < t < +\infty$, with the branch (21a) of the homoclinic solution of problem (19) identified by solid line. This completes the solution of the $O(1)$ approximation of the homoclinic solution of Eqs. (14) and (15).

We now consider the $O(\varepsilon)$ problem, which takes into account (to the first order) the effects of damping. We will be especially interested in studying the perturbation of the homoclinic solution (21a) and (21b) of the $O(1)$ problem when weak damping [of $O(\varepsilon^{1/2})$] is added. The $O(\varepsilon^{1/2})$ analysis will also provide the correction due to damping of the critical value of the impulse (initial condition) corresponding to the perturbed homoclinic solution (cf. Fig. 7).

Substituting Eq. (16) in Eq. (14) and considering $O(\varepsilon^{1/2})$ terms, we derive the following problem at the next order of approximation,

$$\dot{z}_1 - \frac{\mathrm{j}}{2}(z_1^* z_0^2 + 2|z_0|^2 z_1) + \frac{\mathrm{j}}{2}z_1 = -\frac{1}{2}z_0 + \frac{\mathrm{j}B_1}{2}, \quad z_1(0) = B_1. \tag{23}$$

This is a complex quasi-linear ordinary differential equation with a nonhomogeneous term. Although the following analysis applies to the general class of solutions of Eq. (23), from hereon we will focus only on the

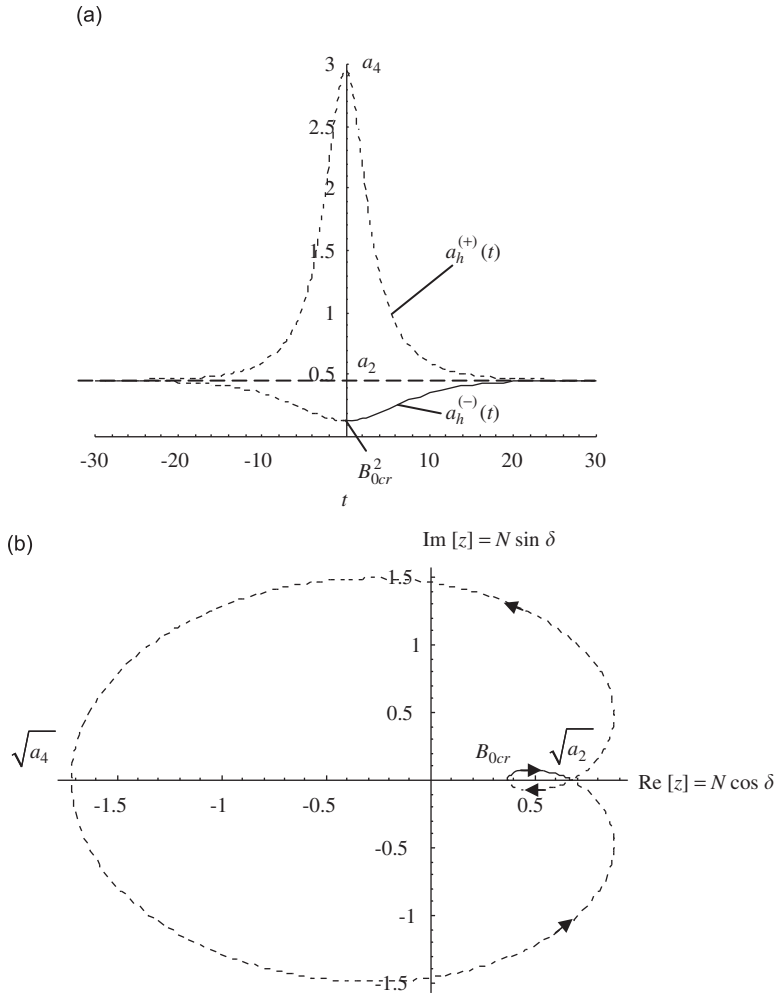

Fig. 9. Homoclinic orbits (21a), (21b), (22a) and (22b): (a) $a_h^{(\pm)}(t)$, (b) parametric plot of Im[z] against Re[z] with t being the parametrizing variable; solid line represents the homoclinic solution of the slow-flow problem (19).

solution corresponding to the perturbation of the homoclinic orbit (21a) and (21b) of the $O(1)$ problem. To this end, the perturbed homoclinic solution $z_{1h}(t)$ of Eq. (23) is written as,

$$z_{1h}(t) = z_{1\mathrm{HS}}(t) + z_{1\mathrm{PI}}(t), \tag{24}$$

i.e., the solution is expressed as a superposition of the general homogeneous solution $z_{1\mathrm{HS}}(t)$ and a particular integral $z_{1\mathrm{PI}}(t)$. Key in solving the problem, is the computation of two linearly independent homogeneous solutions of Eq. (23), since then, a particular integral may be systematically computed by either solving the differential equation satisfied by the Wronskian relation satisfied by the linearly independent homogeneous solutions, or by the employing the method of variation of parameters.

We can easily prove (by simple substitution into the complex homogeneous equation) that one homogeneous solution of Eq. (23) can be computed in terms of the $O(1)$ homoclinic solution $z_{0h}(t)$ as, $z_{1\mathrm{HS}}^{(1)}(t) = \Lambda \dot{z}_{0h}(t)$, $\Lambda \in R$. At this point we decompose the complex solution into real and imaginary parts,

$$z_{1h}(t) = x_{1h}(t) + \mathrm{j}y_{1h}(t), \quad z_{0h}(t) = x_{0h}(t) + \mathrm{j}y_{0h}(t). \tag{25}$$

Then the first homogeneous solution of Eq. (23) is expressed as,

$$\left.\begin{aligned} x_{1\mathrm{HS}}^{(1)}(t) &= \frac{2}{B_{0\mathrm{cr}}}\dot{x}_{0h}(t) \\ y_{1\mathrm{HS}}^{(1)}(t) &= \frac{2}{B_{0\mathrm{cr}}}\dot{y}_{0h}(t) \end{aligned}\right\} \Rightarrow z_{1\mathrm{HS}}^{(1)} = \frac{2}{B_{0\mathrm{cr}}}[\dot{x}_{0h}(t) + \mathrm{j}\dot{y}_{0h}(t)], \tag{26}$$

where the real constant Λ is selected so that the first homogeneous solution satisfies the initial conditions:

$$x_{1\mathrm{HS}}^{(1)}(0) = 0, \quad y_{1\mathrm{HS}}^{(1)}(0) = +1 \;\Rightarrow\; z_{1\mathrm{HS}}^{(1)}(0) = \mathrm{j}.$$

In addition, the homogeneous solution (26) satisfies the limiting conditions $\lim_{t\to+\infty} x_{1\mathrm{HS}}^{(1)}(t) = 0$ and $\lim_{t\to+\infty} y_{1\mathrm{HS}}^{(1)}(t) = 0$.

To compute a second linearly independent homogeneous solution of Eq. (23) it is convenient to carry the entire analysis in the real domain by decomposing Eq. (23) to the following set of two real quasi-linear coupled ordinary differential equations with nonhomogeneous terms:

$$\begin{Bmatrix} \dot{x}_{1h} \\ \dot{y}_{1h} \end{Bmatrix} + \begin{bmatrix} x_{0h}y_{0h} & (x_{0h}^2 + 3y_{0h}^2 - 1)/2 \\ -(3x_{0h}^2 + y_{0h}^2 - 1)/2 & -x_{0h}y_{0h} \end{bmatrix} \begin{Bmatrix} x_{1h} \\ y_{1h} \end{Bmatrix} = \begin{Bmatrix} -x_{0h}/2 \\ (B_{1\mathrm{cr}} - y_{0h})/2 \end{Bmatrix} \tag{27}$$

Note that problem (27) governs the $O(\varepsilon^{1/2})$ perturbation of the $O(1)$ homoclinic solution (21a) and (21b), and that the real constant $B_{1\mathrm{cr}}$ on the right-hand-side denotes the $O(\varepsilon^{1/2})$ correction to $B_{0\mathrm{cr}}$ in Eq. (16). We seek a second homogeneous solution of Eq. (27) satisfying the initial conditions, $x_{1\mathrm{HS}}^{(2)}(0) = -1$, $y_{1\mathrm{HS}}^{(2)}(0) = 0$. Accordingly, we consider the following relation satisfied by the Wronskian of independent homogeneous solutions of Eq. (27):

$$W(t) = x_{1\mathrm{HS}}^{(1)}(t)y_{1\mathrm{HS}}^{(2)}(t) - x_{1\mathrm{HS}}^{(2)}(t)y_{1\mathrm{HS}}^{(1)}(t) \tag{28a}$$

The Wronskian satisfies the following relation,

$$\dot{W}(t) = 0 \;\Rightarrow\; W(t) = W(0) = 1, \tag{28b}$$

from which we conclude that the second homogeneous solution satisfies the relation,

$$x_{1\mathrm{HS}}^{(1)}(t)y_{1\mathrm{HS}}^{(2)}(t) - x_{1\mathrm{HS}}^{(2)}(t)y_{1\mathrm{HS}}^{(1)}(t) = 1 \;\Rightarrow\; x_{1\mathrm{HS}}^{(2)}(t) = \frac{x_{1\mathrm{HS}}^{(1)}(t)y_{1\mathrm{HS}}^{(2)}(t) - 1}{y_{1\mathrm{HS}}^{(1)}(t)}. \tag{29}$$

When this expression is substituted into the second of equations (27) with the nonhomogeneous term dropped, it leads to the first-order quasi-linear differential equation governing $y_{1\mathrm{HS}}^{(2)}$,

$$\dot{y}_{1\mathrm{HS}}^{(2)} + \left[a_{21}\frac{x_{1\mathrm{HS}}^{(1)}}{y_{1\mathrm{HS}}^{(1)}} + a_{22}\right] y_{1\mathrm{HS}}^{(2)} = \frac{a_{21}}{y_{1\mathrm{HS}}^{(1)}}, \quad y_{1\mathrm{HS}}^{(2)}(0) = 0, \tag{30}$$

with $a_{11} = x_{0h}y_{0h}$, $a_{12} = (x_{0h}^2 + 3y_{0h}^2 - 1)/2$, $a_{21} = -(3x_{0h}^2 + y_{0h}^2 - 1)/2$, and $a_{22} = -x_{0h}y_{0h}$. The solution of Eq. (30) provides the second linearly independent homogeneous solution of Eq. (23), which is computed explicitly as,

$$\left.\begin{aligned} x_{1\mathrm{HS}}^{(2)}(t) &= \frac{x_{1\mathrm{HS}}^{(1)}(t)y_{1\mathrm{HS}}^{(2)}(t) - 1}{y_{1\mathrm{HS}}^{(1)}(t)} \\ y_{1\mathrm{HS}}^{(2)}(t) &= \int_0^t \frac{a_{21}(\tau)}{y_{1\mathrm{HS}}^{(1)}(\tau)} \exp\left\{-\int_\tau^t \left[a_{21}(s)\frac{x_{1\mathrm{HS}}^{(1)}(s)}{y_{1\mathrm{HS}}^{(1)}(s)} + a_{22}(s)\right] \mathrm{d}s\right\} \mathrm{d}\tau \end{aligned}\right\} \;\Rightarrow\; z_{1\mathrm{HS}}^{(2)} = x_{1\mathrm{HS}}^{(2)}(t) + \mathrm{j}y_{1\mathrm{HS}}^{(2)}(t). \tag{31}$$

The second homogeneous solution satisfies the initial conditions,

$$x_{1\mathrm{HS}}^{(2)}(0) = -1, \quad y_{1\mathrm{HS}}^{(2)}(0) = 0 \;\Rightarrow\; z_{1\mathrm{HS}}^{(2)}(0) = -1.$$

Contrary to Eq. (26) the second linearly independent solution diverges with time, as $\lim_{t\to+\infty} x^{(2)}_{1\mathrm{HS}}(t) = +\infty$ and $\lim_{t\to+\infty} y^{(2)}_{1\mathrm{HS}}(t) = +\infty$.

Making use of the two linearly independent homogeneous Eqs. (26) and (31) we can compute a first particular integral by the method of variation of parameters. By expressing the real and imaginary parts of the particular integral $z_{1\mathrm{PI}}(t) = x_{1\mathrm{PI}}(t) + jy_{1\mathrm{PI}}(t)$, in the form,

$$\begin{Bmatrix} x_{1\mathrm{PI}}(t) \\ y_{1\mathrm{PI}}(t) \end{Bmatrix} = c_1(t) \begin{Bmatrix} x^{(1)}_{1\mathrm{HS}}(t) \\ y^{(1)}_{1\mathrm{HS}}(t) \end{Bmatrix} + c_2(t) \begin{Bmatrix} x^{(2)}_{1\mathrm{HS}}(t) \\ y^{(2)}_{1\mathrm{HS}}(t) \end{Bmatrix}, \tag{32}$$

and evaluating the real coefficients $c_1(t)$ and $c_2(t)$ by substituting into Eq. (27), we obtain the following explicit general solution of problem (23), providing the $O(\varepsilon^{1/2})$ perturbation of the homoclinic orbit,

$$\begin{Bmatrix} x_{1h}(t) \\ y_{1h}(t) \end{Bmatrix} = \left[\Lambda_1 + \int_0^t \left\{ -\frac{x_{0h}(\tau)}{2} y^{(2)}_{1\mathrm{HS}}(\tau) - \left[\frac{B_{1\mathrm{cr}} - y_{0h}(\tau)}{2} \right] x^{(2)}_{1\mathrm{HS}}(\tau) \right\} \mathrm{d}\tau \right] \begin{Bmatrix} x^{(1)}_{1\mathrm{HS}}(t) \\ y^{(1)}_{1\mathrm{HS}}(t) \end{Bmatrix}$$
$$+ \left[\Lambda_2 + \int_0^t \left\{ \frac{x_{0h}(\tau)}{2} y^{(1)}_{1\mathrm{HS}}(\tau) + \left[\frac{B_{1\mathrm{cr}} - y_{0h}(\tau)}{2} \right] x^{(1)}_{1\mathrm{HS}}(\tau) \right\} \mathrm{d}\tau \right] \begin{Bmatrix} x^{(2)}_{1\mathrm{HS}}(t) \\ y^{(2)}_{1\mathrm{HS}}(t) \end{Bmatrix}. \tag{33}$$

This expression incorporates both the homogeneous solution and the particular integral and contains two unknown real constants Λ_1 and Λ_2 which are evaluated by imposing the initial conditions corresponding to the perturbed homoclinic orbit. Moreover, this expression contains the correction $B_{1\mathrm{cr}}$ to the initial condition for motion on the perturbed homoclinic orbit. By imposing the initial condition of Eq. (23),

$$z_{1h}(0) = B_{1\mathrm{cr}} \quad \Rightarrow \quad x_{1h}(0) = B_{1\mathrm{cr}}, \quad y_{1h}(0) = 0,$$

we compute the two unknown coefficients as

$$\Lambda_1 = 0 \quad \text{and} \quad \Lambda_2 = -B_{1\mathrm{cr}}. \tag{34}$$

Then, taking into account that the components of the second homogeneous solution $x^{(2)}_{1\mathrm{HS}}(t)$ and $y^{(2)}_{1\mathrm{HS}}(t)$ in the second additive term of Eq. (33) diverge as $t \to +\infty$, and imposing the requirement that $x_{1h}(t)$ and $y_{1h}(t)$ should be bounded as $t \to +\infty$, it should be satisfied that

$$-B_{1\mathrm{cr}} + \int_0^{+\infty} \left\{ \frac{x_{0h}(\tau)}{2} y^{(1)}_{1\mathrm{HS}}(\tau) + \left[\frac{B_{1\mathrm{cr}} - y_{0h}(\tau)}{2} \right] x^{(1)}_{1\mathrm{HS}}(\tau) \right\} \mathrm{d}\tau = 0. \tag{35a}$$

This evaluates $B_{1\mathrm{cr}}$ as

$$B_{1\mathrm{cr}} = \frac{\int_0^{+\infty} [x_{0h}(\tau) y^{(1)}_{1\mathrm{HS}}(\tau) - y_{0h}(\tau) x^{(1)}_{1\mathrm{HS}}(\tau)] \, \mathrm{d}\tau}{2 - \int_0^{+\infty} x^{(1)}_{1\mathrm{HS}}(\tau) \, \mathrm{d}\tau}. \tag{35b}$$

This completes the solution of the $O(\varepsilon^{1/2})$ problem (23) and provides the damped perturbation of the homoclinic orbit in the slow flow (14) and (15) with $O(\varepsilon^{1/2})$ damping.

In summary, by applying the complexification-averaging method we have reformulated the system to an equivalent integro-differential equation that governs the slow flow. By a suitable early time approximation of this complex equation we have determined analytically the response of the system near to the homoclinic orbit which defines the critical amount of energy for optimum TET. The analytic approximation of the perturbed homoclinic orbit for time scales of $O(\varepsilon^{-1/2})$ has been proven to be,

$$z_h(t) = z_{0h}(t) + \varepsilon^{1/2} \hat{\lambda} z_{1h}(t) + O(\varepsilon), \quad B_{\mathrm{cr}}(\hat{\lambda}) = B_{0\mathrm{cr}} + \varepsilon^{1/2} \hat{\lambda} B_{1\mathrm{cr}} + O(\varepsilon), \tag{36}$$

where $z_{0h}(t) = \sqrt{a_h^{(-)}(t)} \exp[\delta_h^{(-)}(t)]$ and $a_h^{(-)}(t)$, $\delta_h^{(-)}(t)$ is the analytical homoclinic orbit of the first-order system (undamped) which is computed by Eqs. (21a) and (21b). Additionally, the first order correction with respect to damping $z_{1h}(t) = x_{1h}(t) + \mathrm{j} y_{1h}(t)$, is computed by considering $O(\varepsilon^{1/2})$ terms in our analysis, resulting in $x_{1h}(t)$ and $y_{1h}(t)$ given by Eqs. (33), (34) and (35b). Finally, the critical initial condition $B_{0\mathrm{cr}} \approx 0.36727$ is found by analytically studying the unperturbed homoclinic orbit while the first order correction $B_{1\mathrm{cr}}$

(computed by Eq. (35b)) is derived by imposing the requirements that $x_{1h}(t)$ and $y_{1h}(t)$ should be bounded as $t \to +\infty$.

For $\varepsilon = 0.05$ and $\hat{\lambda} = 0.4472$ we estimate the initial condition as $B_{cr}(\hat{\lambda} = 0.4472) \approx 0.3806$, which compares to the numerical value of 0.3814 derived from the numerical integration of the initial approximation of the slow-flow (14) and (15) (cf. Fig. 7). Taking into account the previous coordinate transformations and introduced rescalings for the initial condition B, the previous analytical result (Eq. (35b)) predicts an initial condition (impulse) of the original problem equal to $X = 0.0983$ for optimal TET (i.e., for the excitation of the damped homoclinic perturbation), compared to the numerical result of $X = 0.1099$ derived from simulation of the full averaged slow-flow (9) (cf. Fig. 5d); we note that the error is of $O(\varepsilon = 0.05)$ and compatible to our previous asymptotic derivations. Based on the previous analytical result (Eq. (35b)) an optimal choice of system parameters can be made for a given energy level so that optimal TET is performed for a typical system response (a response with initial energy close to the given one).

In Fig. 10a we provide a comparison of the three approximate models for the slow-flow dynamics in the regime of optimal TET. The asymptotic analysis correctly predicts the half-cycle "super-slow" transfer of

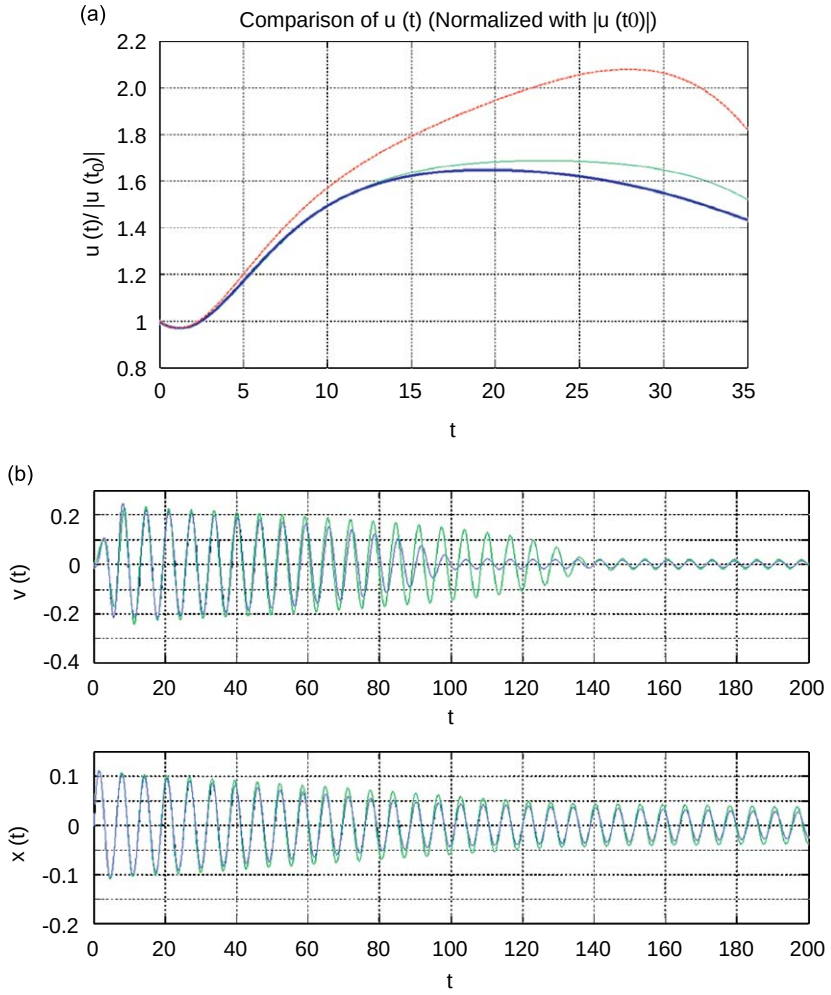

Fig. 10. (a) Slow-flow response in the regime of optimal TET ('super-slow' half-cycle of TET), for $\varepsilon = 0.05$, $C = 1$ and $\lambda = \varepsilon^{1/2}\hat{\lambda} = 0.1$; comparison of full slow-slow (7) or (9) - - - - -, with the approximation of the slow-flow in the initial stage of the dynamics (12) or (14) ——, and of the asymptotic solution (36)—. (b) Comparison of the full averaged system (7) or (9) ——, with the original system (1) —— in the regime of optimal TET.

energy from the LO to the NES in the initial regime of the motion, although it underestimates the maximum amplitude of the response during this half-cycle; this can be explained by the fact that the slow-flow approximation (12) or (14) is only valid in the initial regime of the motion. Furthermore, the validity of the averaged system (9) is illustrated in Fig. 10b where a direct comparison of system (1) response with the full averaged system (9) is shown.

This completes the analytical study of the regime of optimal TET in system (4) when intermediate-energy damped IOs are excited. In Figs. 11–13 we study TET in system (4) for excitation of intermediate-energy damped IOs over a wider range of mass asymmetry ε and damping $\varepsilon\lambda$. These plots were derived by direct numerical integrations of the differential equations of motion, and monitoring the instantaneous energy of the system versus time. Numerical results indicate that, by increasing ε (i.e., by decreasing the mass asymmetry) and the damping coefficient $\varepsilon\lambda$, the capacity of the NES for optimal TET also deteriorates. This is due to the fact that by increasing the inertia of the NES the amplitude of the relative response between the LO and the NES is expected to decrease, which hinders the capacity of the damper of the NES to effectively dissipate vibration energy. Moreover, by increasing damping in the system, the damper of the LO dissipates an increasingly higher portion of the vibration energy which leads to deterioration of TET; this markedly slows energy dissipation in the system, as judged by comparing the times required for energy dissipation in the plots of Fig. 13 to the corresponding times in the regimes of optimal TET in the plots of Figs. 11 and 12.

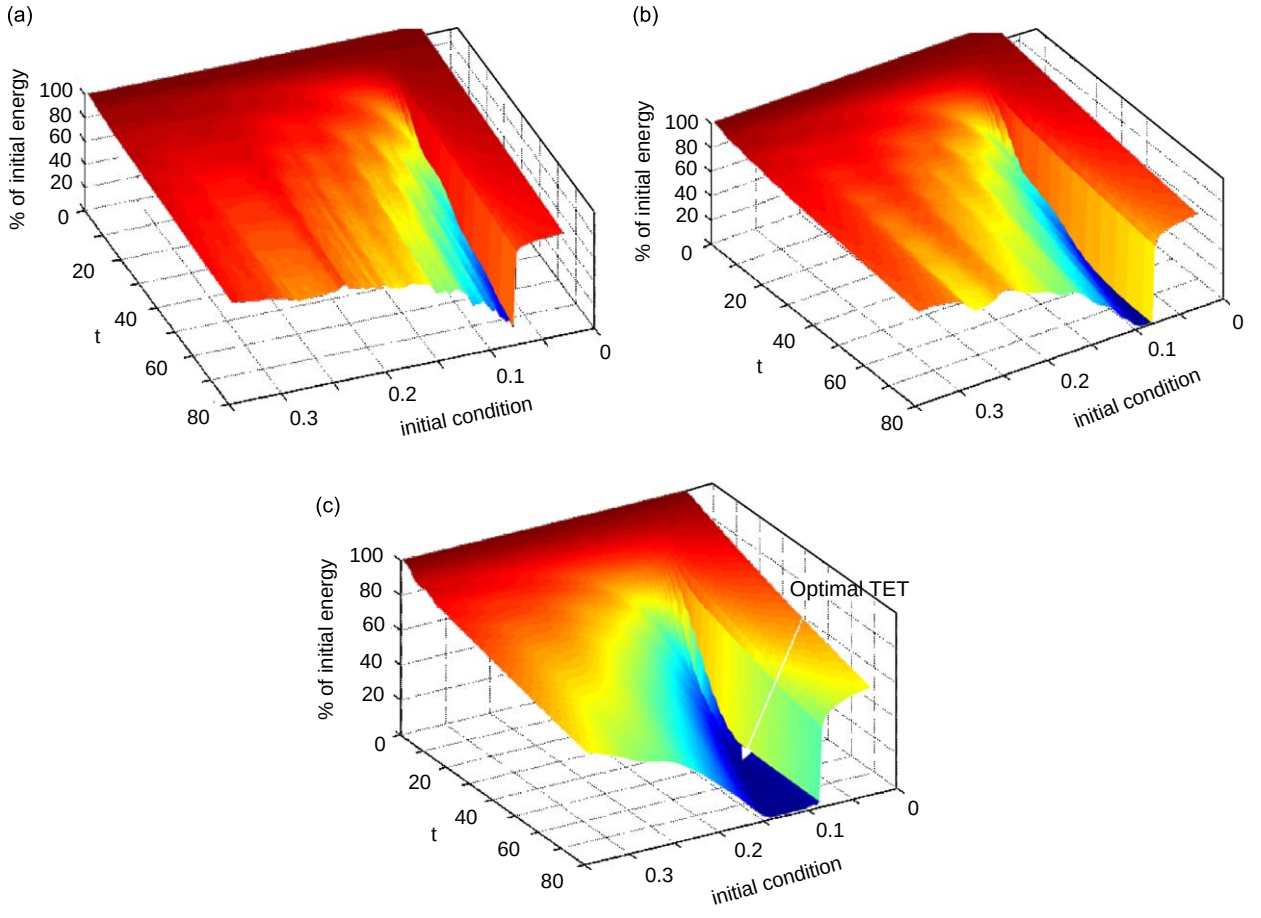

Fig. 11. Energy dissipation in system (4) when damped IOs are excited for mass asymmetry $\varepsilon = 0.03$: (a) $\varepsilon\lambda = 0.015$, (b) $\varepsilon\lambda = 0.003$ and (c) $\varepsilon\lambda = 0.006$.

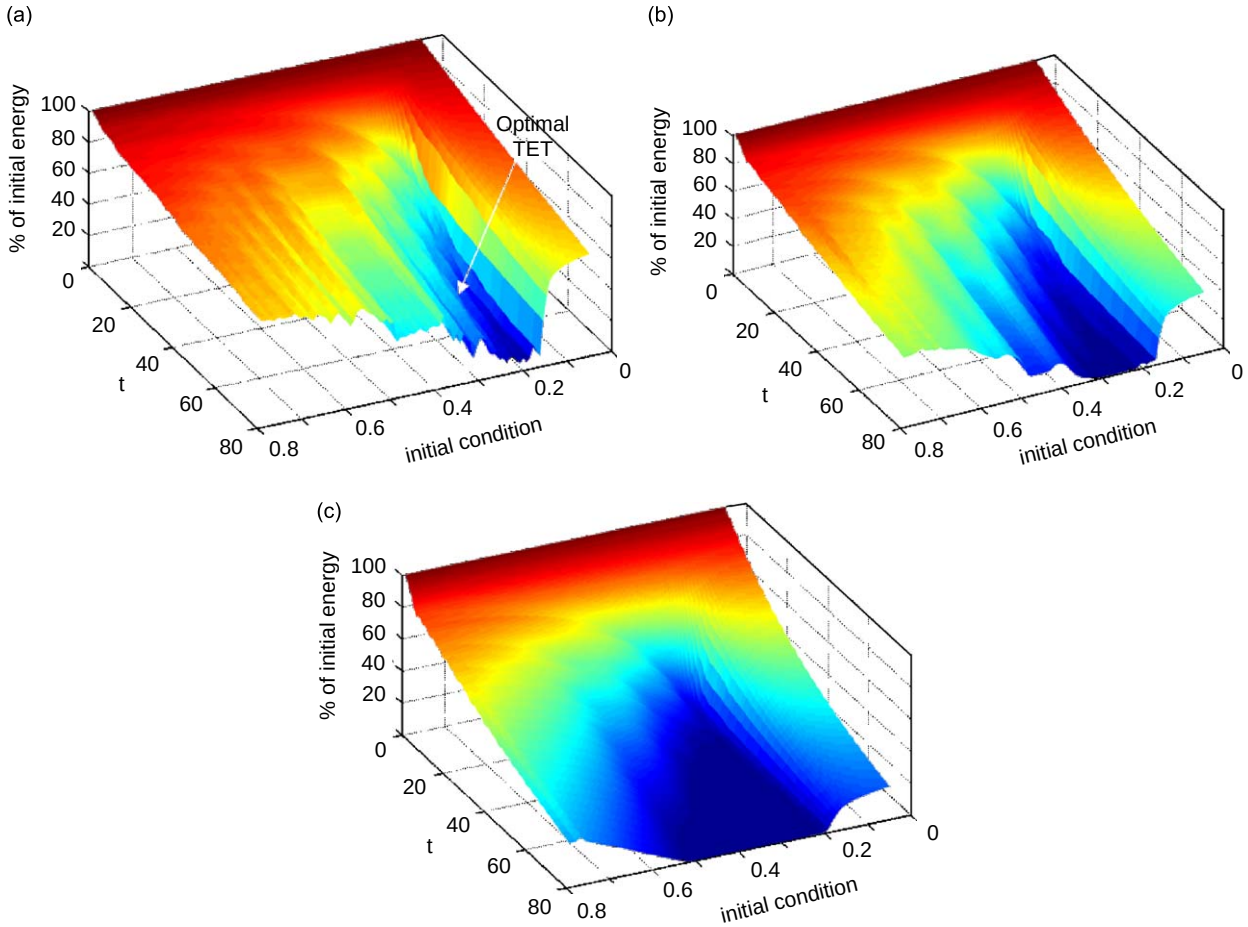

Fig. 12. Energy dissipation in system (4) when damped IOs are excited for mass asymmetry $\varepsilon = 0.1$: (a) $\varepsilon\lambda = 0.005$, (b) $\varepsilon\lambda = 0.01$ and (c) $\varepsilon\lambda = 0.02$.

4. Concluding remarks

We have studied TET in coupled nonlinear oscillators associated with 1:1 resonance capture. Referring to system (4), the dynamics (and TET) depends on the damping coefficient λ and the parameter ε that scales the mass of the NES and damping. In Part I of this work [14] the dynamics was examined under the assumption that λ is small and ε arbitrary. In Part II we assumed that ε is small; although λ was selected to be of $O(\varepsilon^{1/2})$, this was not necessary in our study of the perturbation of the homoclinic orbit in the regime of optimal TET. Hence, the analysis of this work can be extended (with some modification) to the case of arbitrary λ.

We showed that in the weakly damped system, optimal TET is realized for initial energies where the excited damped IOs are in the neighborhood of the homoclinic orbit of the unstable out-of-phase damped invariant manifold $S11-$; in the underlying Hamiltonian system this unstable periodic orbit is generated at a critical energy through a saddle-node bifurcation. We studied analytically the perturbation of the homoclinic orbit in the weakly damped system, which introduces an additional slow-time scale in the averaged dynamics and leads to optimal TET from the LO to the NES in a single "super-slow" half-cycle. At higher energies, this "super-slow" half-cycle is replaced by strong nonlinear beats (these are generated from the attraction of the dynamics to the stable in-phase damped orbit $S11+$). Although producing significant TET through nonlinear beats, this TET is not optimal. At lower energies than the one corresponding to the optimal TET regime, the dynamics is attracted by the stable, weakly nonlinear (linearized), out-of-phase damped orbit $S11-$ and TET is negligible.

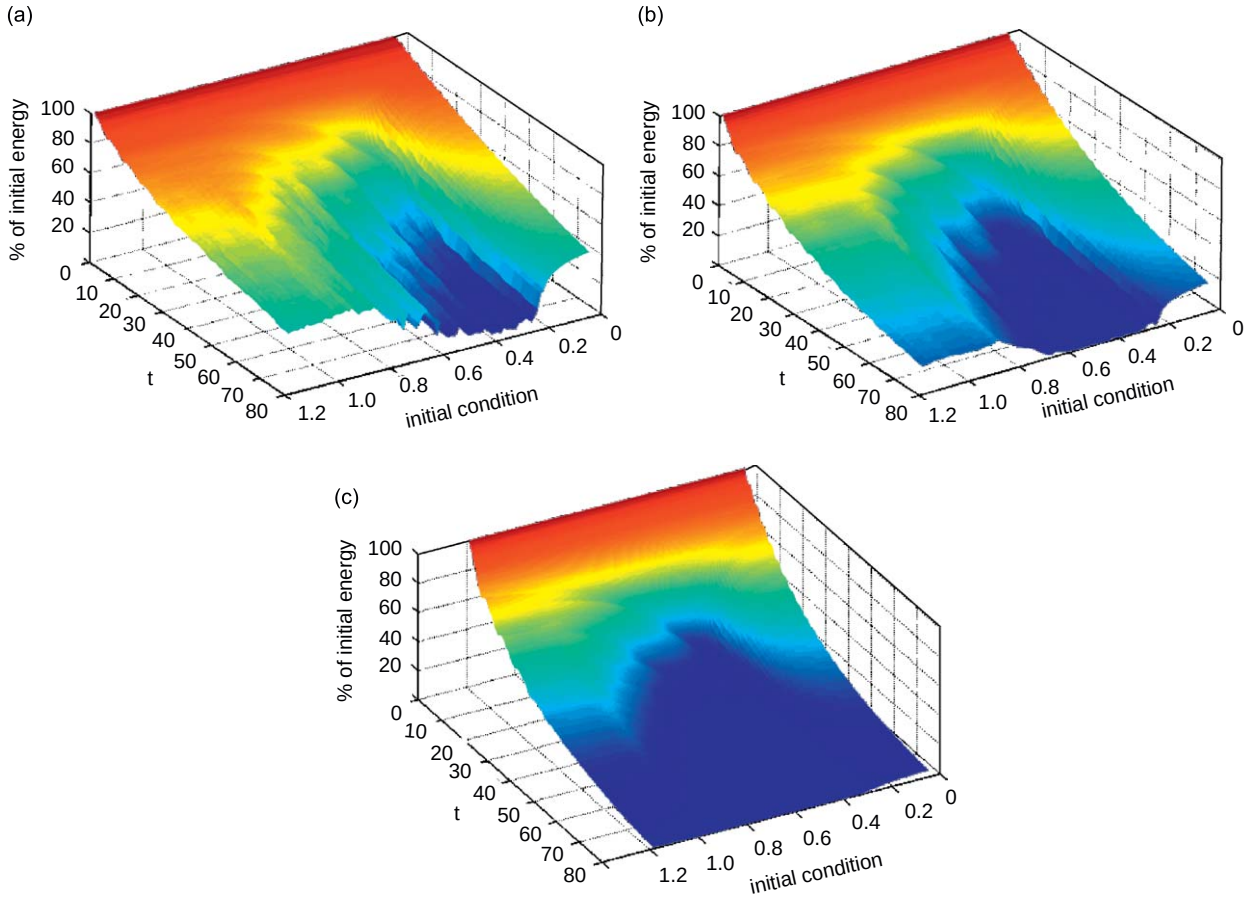

Fig. 13. Energy dissipation in system (4) when damped IOs are excited for mass asymmetry $\varepsilon = 0.2$: (a) $\varepsilon\lambda = 0.01$, (b) $\varepsilon\lambda = 0.02$ and (c) $\varepsilon\lambda = 0.04$.

The aforementioned conclusions are valid for the weakly damped system (4), under the assumption of sufficiently small ε; i.e., for a lightweight NES in a system with high mass asymmetry.

References

[1] V.I. Arnold, *Dynamical Systems III, Encyclopedia of Mathematical Sciences*, Vol. 3, Springer Verlag, Berlin and New York, 1988.
[2] D.D. Quinn, R.H. Rand, J. Bridge, The dynamics of resonance capture, *Nonlinear Dynamics* 8 (1995) 1–20.
[3] G. Kopidakis, S. Aubry, G.P. Tsironis, Targeted energy transfer through discrete breathers in nonlinear systems, *Physical Review Letters* 87 (2001) paper 165501.
[4] S. Aubry, S. Kopidakis, A.M. Morgante, G.P. Tsironis, Analytic conditions for targeted energy transfer between nonlinear oscillators or discrete breathers, *Physica B* 296 (2001) 222–236.
[5] A.M. Morgante, M. Johansson, S. Aubry, G. Kopidakis, Breather-phonon resonances in finite-size lattices: phantom breathers, *Journal of Physics A* 35 (2002) 4999–5021.
[6] D.L. Vainchtein, E.V. Rovinsky, L.M. Zelenyi, A.I. Neishtadt, Resonances and particle stochastization in nonhomogeneous electromagnetic fields, *Journal of Nonlinear Science* 14 (2004) 173–205.
[7] K.R. Khusnutdinova, D.E. Pelinovsky, On the exchange of energy in coupled Klein–Gordon oscillators, *Wave Motion* 38 (2003) 1–10.
[8] P. Maniadis, G. Kopidakis, S. Aubry, Classical and quantum targeted energy transfer between nonlinear oscillators, *Physica D* 188 (2004) 153–177.
[9] C.W. Cai, H.C. Chan, Y.K. Cheung, Localized modes in a two-degree-coupled periodic system with a nonlinear disordered subsystem, *Chaos, Solitons and Fractals* 11 (2000) 1481–1492.

[10] P. Malatkar, A.H. Nayfeh, On the transfer of energy between widely spaced modes in structures, *Nonlinear Dynamics* 31 (2003) 225–242.
[11] S.J. Zhu, Y.F. Zheng, Y.M. Fu, Analysis of nonlinear dynamics of a two-degree-of-freedom vibration system with nonlinear damping and nonlinear spring, *Journal of Sound and Vibration* 271 (2004) 15–24.
[12] O.V. Gendelman, D.V. Gorlov, L.I. Manevitch, A.I. Musienko, Dynamics of coupled linear and essentially nonlinear oscillator with substantially different masses, *Journal of Sound and Vibration* 286 (2005) 1–19.
[13] G. Kerschen, Y.S. Lee, A.F. Vakakis, D.M. McFarland, L.A. Bergman, Irreversible passive energy transfer in coupled oscillators with essential nonlinearity, *SIAM Journal of Applied Mathematics* 66 (2006) 648–679.
[14] D.D. Quinn, O.V. Gendelman, G. Kerschen, T.P. Sapsis, L.A. Bergman, A.F. Vakakis, Efficiency of targeted energy transfers in coupled nonlinear oscillators associated with 1:1 resonance captures: part I, *Journal of Sound and Vibration* 311 (2008) 1228–1248.
[15] G. Kerschen, O.V. Gendelman, A.F. Vakakis, L.A. Bergman, D.M. McFarland, Impulsive periodic and quasi-periodic orbits in coupled oscillators with essential nonlinearity, *Communication in Nonlinear Science and Numerical Simulation* 13 (2008) 959–978.
[16] L.I. Manevitch, *Complex Representation of Dynamics of Coupled Oscillators in Mathematical Models of Nonlinear Excitations, Transfer Dynamics and Control in Condensed Systems*, Kluwer Academic/Plenum Publishers, New York, 1999, pp. 269–300.
[17] L.I. Manevitch, E. Gourdon, C.H. Lamarque, Towards the design of an optimal energetic sink in a strongly inhomogeneous two-degree-of-freedom system, *Journal of Applied Mechanics* 74 (2007) 1078–1086.
[18] S.W. Shaw, C. Pierre, Nonlinear normal modes and invariant manifolds, *Journal of Sound and Vibration* 150 (1991) 170–173.
[19] S.W. Shaw, C. Pierre, Normal modes for nonlinear vibratory systems, *Journal of Sound and Vibration* 164 (1993) 85–124.
[20] I.S. Gradshteyn, I.M. Ryzhik, *Table of Integrals, Series and Products*, Academic Press, New York, 1980.